CHALMERS
UNIVERSITY OF TECHNOLOGY

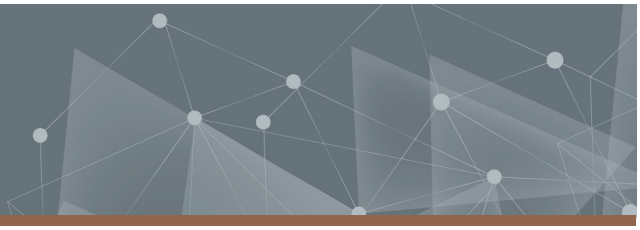

# Assessing potential causality between blood metabolites and primary sclerosing cholangitis using two-sample Mendelian randomization

Master's thesis in Life Sciences

OLA ROSENGREN

Department of Life Sciences
CHALMERS UNIVERSITY OF TECHNOLOGY
UNIVERSITY OF GOTHENBURG
Gothenburg, Sweden 2026

Master's thesis 2026

# Assessing potential causality between blood metabolites and primary sclerosing cholangitis using two-sample Mendelian randomization

Ola Rosengren


CHALMERS
UNIVERSITY OF TECHNOLOGY

Department of Life Sciences
Chalmers University of Technology
University of Gothenburg
Gothenburg, Sweden 2026

Assessing potential causality between blood metabolites and primary sclerosing cholangitis using two-sample Mendelian randomization
OLA ROSENGREN



Supervisors: Pol Solé Navais, Department of Molecular and Clinical Medicine, Sahlgrenska University Hospital
Antonio Molinaro, Department of Molecular and Clinical Medicine, Sahlgrenska University Hospital
Examiner: Johan Bengtsson Palme, Department of Life Sciences, Chalmers University of Technology

Master's Thesis 2026
Department of Life Sciences
Chalmers University of Technology and University of Gothenburg
SE-412 96 Gothenburg
Telephone +46 31 772 1000

Typeset in LaTeX
Gothenburg, Sweden 2026

Assessing potential causality between blood metabolites and primary sclerosing cholangitis using two-sample Mendelian randomization

OLA ROSENGREN
Department of Life Sciences
Chalmers University of Technology and University of Gothenburg

# Abstract

Primary sclerosing cholangitis (PSC) is a chronic cholestatic liver disease with a poorly understood aetiology. An observational study by Molinaro et al. have suggested an association between blood circulating metabolites and PSC, however, causal inference is limited by confounding and reverse causation.

The aim of this study was to assess potential causal effects of blood circulating metabolites on PSC risk using Mendelian randomization (MR), and to compare the findings to the associations found in the observational study.

A two-sample MR framework was applied using summary statistics from genome-wide association studies (GWAS) of PSC-associated metabolites and PSC. Instrumental variables (IVs) were selected based on genome-wide significance and linkage disequilibrium pruning. Causal effects were estimated using the inverse variance weighted method, with sensitivity analysis performed to assess heterogeneity and horizontal pleiotropy.

MR analysis were conducted for seven metabolites previously associated with PSC and seven control metabolites with no association. Overall, the selected IVs explained only a small proportion of variance in metabolite levels, as reflected by low F-statistics, indicating weak instrument strength and a potential bias of causal effect estimates towards the null. No evidence of a causal effect was detected for either PSC-associated metabolites nor the control metabolites. Sensitivity analysis indicated moderate heterogeneity with little evidence of horizontal pleiotropy.

These findings suggest that currently available IVs for the blood circulating metabolites are insufficient to robustly assess causality in PSC. While no causal effects were detected, this study highlights important limitations in metabolite-based MR and underscores the need for larger and more powerful metabolite GWAS to enable reliable causal inference.

Keywords: primary sclerosing cholangitis, mendelian randomization, two-sample mendelian randomization, blood circulating metabolites, genome-wide assocation study, instrumental variables, causal inference

# Acknowledgements

First and foremost, I would like to express my sincere gratitude to my supervisors, Pol Solé Navais and Antonio Molinaro, for the opportunity to be part of the Wallenberg Laboratory for Cardiovascular and Metabolic Research. I am especially grateful to my primary supervisor, Pol, for your continuous support, guidance, and encouragement throughout this project, even during your busiest periods. Your availability and willingness to help have been invaluable. I would also like to thank the people at the Wallenberg Laboratory for creating such a welcoming and stimulating environment, your presence has been invaluable.

Ola Rosengren, Gothenburg, April 2026

# Contents

# List of Figures

# List of Tables

# List of Acronyms

| | |
|---|---|
| $\lambda_{GC}$ | $\lambda$ genomic control |
| EAF plot | Effect allele frequency plot |
| GWAS | Genome-wide association study |
| HLA | Human leukocyte antigen |
| HRC | Haplotype reference consortium |
| IBD | Inflammatory bowel disease |
| IV | Instrumental variable |
| IVW | Inverse variance weighted |
| LD | Linkage disequilibrium |
| MAF | Minor allele frequency |
| MR | Mendelian randomization |
| PSC | Primary sclerosing cholangitis |
| Q-Q plot | Quantile-Quantile plot |
| QC | Quality control |
| RCT | Randomized controlled trial |
| SNP | Single nucleotide polymorphism |
| UDCA | Ursodeoxycholic acid |

# 1

# Introduction

Primary sclerosing cholangitis (PSC) is a chronic liver disease characterized by progressive inflammation and fibrosis of the bile ducts, often leading to liver failure and the need for transplantation. Despite its clinical severity, the underlying mechanisms of disease development remain poorly understood, and effective medical treatments are limited [1].

A recent study have identified a number of blood circulating metabolites that differ significantly between individuals with PSC and healthy controls [2]. However, these findings are based on observational data and therefore cannot determine whether these metabolic alterations contribute to disease development or arise as a consequence of the disease. This limitation highlights the need for approaches that can distinguish causal relationships from correlation.

Genetic variants, which are randomly allocated at conception, provide an opportunity to address this challenge. Mendelian Randomization (MR) uses such variants as instrumental variables (IVs) to infer causal effects between exposures and outcomes, reducing bias from confounding and reverse causation [3].

## 1.1 Aim

The aim of this project is to investigate whether specific blood-derived metabolites have a causal effect on the risk of PSC using a two-sample MR framework. By integrating genome-wide association study (GWAS) summary statistics for metabolites and PSC, and applying sensitivity analyses, this study seeks to provide robust evidence for or against a causal role of these metabolites in PSC.

# 2

# Theory

In this section, the biological and methodological background relevant to this study is presented. This includes an overview on PSC, challenges in observational causal inference, the principles of MR, and the current understanding of the genetic architecture of PSC.

## 2.1 Introduction to PSC

Primary sclerosing cholangitis (PSC) is a rare, progressive liver disease characterized by chronic inflammation and scarring of the bile ducts [1]. The role of the bile duct is to transport the digestive liquid, bile, from the liver to the small intestine [4]. The inflammation in the bile duct caused by PSC leads to scar formation, narrowing the bile duct, which causes gradual damage to the liver [1].

The cause of PSC is not understood, moreover, there is no established treatment. A well studied candidate as a drug is ursodeoxycholic acid (UDCA), with some studies suggesting it can improve symptoms and survival. However, there are conflicting guidelines on how or whether it is to be used [1]. As for surgical options, either biliary reconstructive procedures or liver transplantation can be done. However, even with a major intervention like liver transplantation, up to 20 to 40% of patients develop reccurring PSC [5]. Furthermore, PSC is a premalignant disease, with 10 to 20% of patients developing bile duct cancer [1].

### 2.1.1 Metabolites associated to PSC

At Wallenberg Laboratory, Sahlgrenska Academy, Molinaro et al. have identified a number of blood derived metabolites, using a non-targeted approach, which are significantly differentially abundant in subjects with PSC compared with those without (Table 2.1) [2].

**Table 2.1:** List of metabolites found to be associated with PSC by Molinaro et al. In addition, the table contains metabolites that Molinaro et al. found to have no association to PSC, which are used as negative controls in this [2].

| Metabolite | Super-pathway | Sub-pathway |
|---|---|---|
| **PSC-associated metabolites** | | |
| Imidazole propionate | Amino acids | Histidine metabolism |
| Pyroglutamine | Amino acids | Glutamate metabolism |
| 3-methyl-2-oxovalerate | Amino acids | Leucine, Isoleucine and valine metabolism |
| 4-methyl-2-oxopentanoate | Amino acids | Leucine, isoleucine and valine metabolism |
| Oxalate (ethanedioate) | Cofactors and vitamins | Ascorbate and aldarate metabolism |
| Threonate | Cofactors and vitamins | Ascorbate and aldarate metabolism |
| Pimeloylcarnitine/3-methyladipoylcarnitine (C7-DC) | Lipids | Fatty acid metabolism (acyl carnitine, dicarboxylate) |
| **Non-associated metabolites** | | |
| Phenylacetate | Amino acids | Phenylalanine metabolism |
| Citrulline | Amino acids | Urea cycle; arginine and proline Metabolism |
| Maltose | Carbohydrates | Glycogen metabolism |
| Arabinose | Carbohydrates | Pentose metabolism |
| Succinoyltaurine | Amino acids | Methionine, cysteine, SAM and taurine metabolism |
| Octanoylcarnitine (C8) | Lipids | Fatty acid metabolism (acyl carnitine, medium chain) |
| Phenyllactate (PLA) | Amino acids | Phenylalanine metabolism |

## 2.2 Challenges in observational causal inference

Although substantial progress has been made in describing the clinical and biological features of PSC, the underlying causal mechanisms driving disease onset and progression remain poorly understood [6]. Previous observational studies investigating potential risk factors, such as inflammatory bowel disease (IBD), for PSC have identified associations, but they are limited in their ability to establish causal relationships, in part due to residual confounding and the possibility of reverse causation [7, 8].

### 2.2.1 Confounding

An observed association between an exposure, such as a risk-factor for a disease, and an outcome, such as a disease, does not necessarily imply a true causal relationship, and confounding is a major source of bias in observational studies. Confounding arises when a third variable is associated with both the exposure and the outcome, creating an illusion of an association. These variables, such as behavioural and societal factors, are often very hard to quantify, which is why confounding is difficult to deal with. In the context of PSC, confounding can obscure the true relationship between potential risk factors, and disease onset, complicating efforts to identify causal mechanisms [8].

### 2.2.2 Reverse causation

An observed association between an exposure and disease may not indicate that the exposure causes the disease and rather, the disease may lead to changes in the exposure. This is known as reverse causation: what appears as a risk factor might instead be a consequence of pre-existing disease [9]. In some cases, the likely direction of causality can be inferred using temporal information, since a cause must precede its effect, or through established biological knowledge of disease mechanisms [8].

## 2.3 Introduction to Mendelian Randomization

Mendelian randomization (MR) is an analytical framework designed to strengthen causal inference in observational studies by reducing bias from confounding and reverse causation. MR uses genetic variants as instruments, to proxy an exposure to assess whether the relationship between an exposure and an outcome is causal. This approach is based on the principle that genetic variants are randomly assigned at conception, in line with Mendel's law of inheritance. The random allocation of genetic variants mimics the design of randomized controlled trials (RCT), thus reducing the risk of environmental confounding and reverse causation [3].

In MR, typically single nucleotide polymorphisms (SNPs), serve as proxies for modifiable exposures. By comparing the associations between SNPs and the exposure with the associations between the same SNPs and the outcome, it is possible to estimate the causal effect of the exposure on the outcome [3].

### 2.3.1 Genome-wide association studies provide associations between SNPs and phenotypes

MR relies on the identification of SNPs that are robustly associated with the exposure of interest[3]. These associations are typically obtained from genome-wide association

studies (GWAS), which tests millions of SNPs across the genome for associations with phenotypic traits in large populations. GWAS provide summary statistics for each SNP, including effect sizes and standard errors, which quantify the strength and direction of association with a given phenotype. These summary-level data form the basis for MR analyses, enabling causal inference without requiring access to individual-level data [10].

### 2.3.2 Two-sample Mendelian Randomization

Two-sample Mendelian randomization estimates causal effects by combining summary statistics from two independent GWAS: one for the exposure and one for the outcome. SNPs that are robustly associated with the exposure are first selected as IVs. For each IV, the estimated effect on the exposure and the estimated effect on the outcome are obtained from the respective GWAS [11].

The causal effect of the exposure on the outcome is then inferred by relating the SNP–outcome association to the SNP–exposure association, typically using a ratio estimate for each variant. These variant-specific estimates are subsequently combined using methods such as inverse-variance weighted (IVW) regression, which provides an overall causal estimate under the assumption that all IVs are valid. Sensitivity analyses, such as MR-Egger, can be applied to assess robustness to potential violations of IV assumptions [11].

A two-sample MR framework is used in this study because it enables the use of large, non-overlapping GWAS consortia for both exposures and outcomes, thereby increasing statistical power and reducing bias from weak IVs and sample overlap.

### 2.3.3 Core assumptions of Mendelian Randomization

However, the causal inference is only valid if certain conditions, known as the core assumptions of MR, are met (Fig. 2.1). These assumptions ensure that the SNPs used as IVs can reliably proxy the exposure without introducing bias. The three key assumptions are:

1) **Relevance**
   Genetic variants are strongly associated with the exposure.

2) **Exchangeability**
   Genetic variants are not associated with confounders of the exposure-outcome relationship.

3) **Exclusion restriction**
Genetic variants affect the outcome only through the exposure, not via other pathways [12].

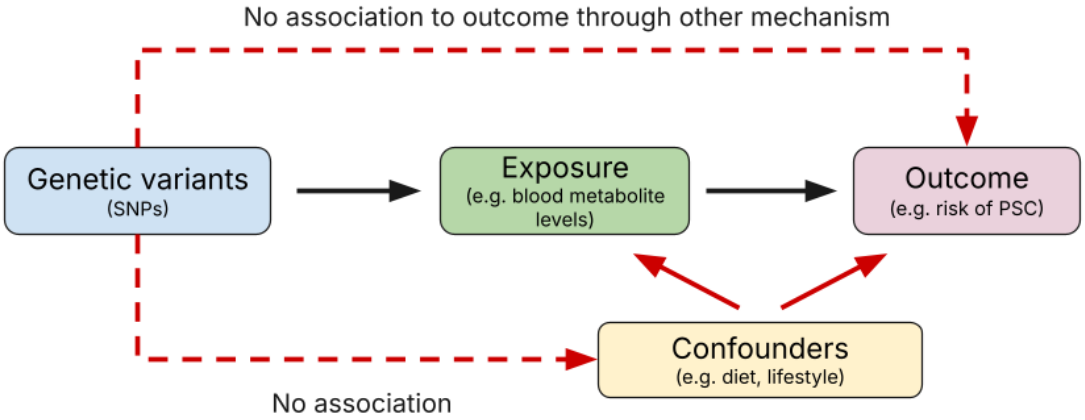


**Figure 2.1:** Ensuring that the three core assumptions hold implies that the genetic variants used as proxies for the exposure influence the outcome only through the exposure itself. The effect of the pathways indicated with red arrows in the figure are thus minimized. If these assumptions are violated, the causal effect estimate may reflect alternative pathways affecting the outcome phenotype rather than the exposure of interest.

### 2.3.4 Instrumental variable selection

Being selective when choosing IVs is crucial to ensure that the IVs are relevant to the exposure as described in section 2.3.3. The conventional approach is to remove non-significant SNPs according to a genome-wide threshold ($p < 5 \cdot 10^{-8}$). This commonly used threshold is derived by controlling for multiple testing in one million independent SNPs [13, 14]. Another approach is to use SNPs that have a known biological association to the exposure as IVs [3].

### 2.3.5 Limitations of MR

MR relied heavily on the three core assumption for a reliable result from the MR analysis. While these can be and extensively should be assessed for (see 3.7.1.1 in the Methods section), they can not be totally accounted for. There can always be some error which can scew and make the results unreliable.

#### 2.3.5.1 Horizontal pleiotropy

Genetic variants are not limited to affecting a single trait, but can independently alter multiple traits, a phenomenon known as horizontal pleiotropy. This can violate

core assumption 3), as the IV may influence the outcome through pathways other than the exposure of interest. In such cases, the estimated causal effect may be biased, as the IV is no longer acting exclusively through the specified exposure [3].

#### 2.3.5.2 Heterogeneity in causal effect estimates

Heterogeneity in causal effect estimates refers to substantial variation in the estimated causal effects across individual SNPs. This may indicate that not all SNPs are valid IVs, either for biological or non-biological reasons. Biological heterogeneity can arise when SNPs influence the exposure through different underlying pathways, leading to varying downstream effects on the outcome, whereas non-biological sources may include violations of MR assumptions such as horizontal pleiotropy. As a result, high heterogeneity can reduce confidence in the overall causal effect estimate and suggests that results should be interpreted with caution [3].

#### 2.3.5.3 Instrumental variable strength

Even if a SNP reaches genome-wide significance, it may not strongly or reliably explain variation in the exposure. Weak IVs can lead to biased and imprecise causal effect estimates, particularly in the presence of measurement error or sample overlap. IV strength is therefore an important consideration in MR, as insufficiently strong IVs can undermine the validity of the analysis. This is often assessed using measures such as the F-statistic, where low values indicate weak IV bias [3].

## 2.4 Genetic basis of PSC

Environmental and immunological factors are thought to contribute to disease development of PSC, however, substantial evidence indicates that genetic factors play an important role in susceptibility to PSC [1]. This section summarizes current knowledge of the genetic architecture of PSC, including evidence for heritability, key loci identified through GWAS, and the extent to which genetic variation explains disease risk.

### 2.4.1 Evidence for heritability

One line of evidence supporting a genetic contribution to PSC comes from studies of familial aggregation. If genetic factors influence disease susceptibility, individuals with affected relatives would be expected to have an increased risk of developing PSC. epidemiological studies demonstrating an increased prevalence of PSC among first-degree relatives of affected individuals. In particular, Bergquist et al. reported that first-degree relatives of PSC patients have a 100-fold increase risk of developing

PSC in comparison with the general population, indicating familial clustering of the disease [15].

While familial aggregation provides indirect evidence of a genetic contribution to PSC, heritability estimates offer a quantitative measure of the proportion of disease risk attributable to genetic variation. Heritability is defined as the proportion of phenotypic variance in a population that can be explained by genetic factors. Estimates from genome-wide association studies indicate that a fraction of PSC susceptibility is genetically determined. Common genetic variants captured by GWAS have been estimated to explain approximately 15% of the overall disease liability [16]. The presence of measurable genetic heritability provides a key prerequisite for MR analyses, as it implies that genetic variants can serve as informative IVs for studying biological causal relationships, such as blood circulating metabolites, and PSC risk.

### 2.4.2 Genetic risk loci for primary sclerosing cholangitis

The strongest and most consistently replicated genetic associations with PSC are located within the human leukocyte antigen (HLA) region on chromosome 6. The HLA region encodes molecules that play a central role in antigen presentation and the regulation of adaptive immune responses [17].

In addition to the strong associations observed within the HLA region, genome-wide association studies have identified multiple non-HLA loci associated with PSC susceptibility. To date, 22 non-HLA genetic loci have been reported [17].

These loci individually confer modest effects on disease risk, but collectively contribute to the polygenic nature of PSC [16]. Many of the identified variants are located near genes involved in immune-related pathways, supporting the hypothesis that PSC is driven by dysregulated immune responses [17].

Despite these discoveries, the identified genetic variants explain only a fraction of the total disease risk [16, 18], indicating that additional genetic and environmental factors remain to be identified. The presence of multiple independent genetic signals influencing disease susceptibility supports the use of genetic variants as IVs in MR analyses to investigate potential causal pathways [19].

# 3

# Methods

This section contains an explanation of the complete pipeline, starting from collection of data to obtaining causal effect estimates for the metabolites on PSC. The aim to provide an overview of the pipeline as well as to explain the methodology in detail step by step.

## 3.1 Study design overview

The workflow is separated into 7 distinct steps (Fig. 3.1). The first 4 steps constitutes the preparation of the GWAS datasets for the MR analysis.

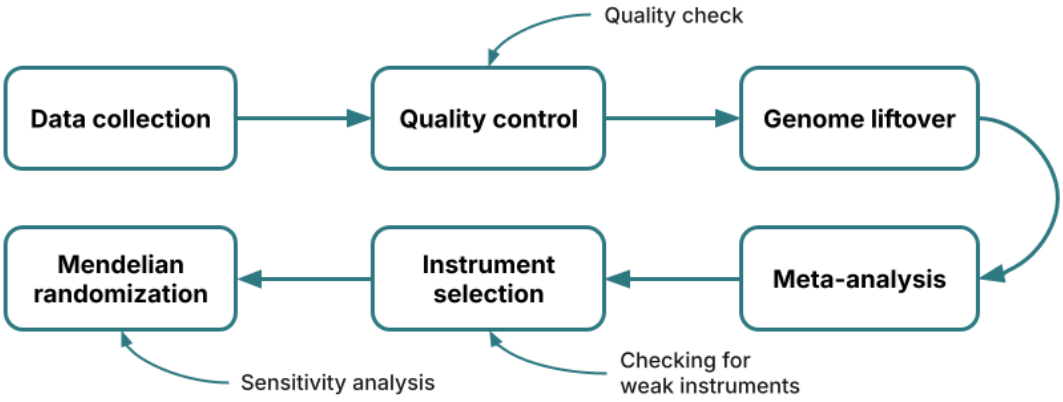


**Figure 3.1:** Overview of the , with indications on which steps additional tests are made on the datasets to identify the quality of the data and the results.

Apart from the 7 PSC-associated metabolites described in section 2.1.1, 7 non-associated metabolites are included as a negative control. In the following sections the steps in the pipeline is explained in more detail. Furthermore, the pipeline is run with the meta-analysis step as well as without, yielding MR results for combined datsets as well as individual datasets for each metabolites.

## 3.2 Data sources

GWAS summary statistics for the metabolites as well as for PSC were collected from GWAS catalog, a databank where GWAS summary statistics are publicly available.

The only exception is the PSC GWAS done on the Finngen cohort, which was accessed directly from the finngen website.

To avoid bias from population stratification, only GWAS done on cohorts of European ancestries were included in this analysis. Moreover, only studies that examined single phenotypes, in order to exclude biases introduced from unwanted phenotypes.

## 3.3 Quality control

The initial step after obtaining the GWAS summary statistics is to perform rigorous quality control (QC). This step is essential to ensure that the data used in the MR analysis are reliable, consistent, and free from technical artifacts or bias. Poorly filtered summary statistics can lead to incorrect effect estimates, weak IVs, or violations of MR assumptions, ultimately compromising the validity of the findings. The QC performed on the GWAS summary statistics is adapted from the protocol presented by Wrinkler et al. in the article *Quality control and conduct of genome-wide association meta-analyses* [20]. The QC workflow includes the following steps:

1) **Standardizing column names**
   Across all datasets the naming of columns is not consistent. Since all datasets will go through the same pipeline it is essential that all necessary column are present and with the same name.

2) **Filter monomorphic SNPs**
   Monomorphic alleles have an allele frequency of =0 or =1, meaning that all individuals have the same allele. Thus comparison between alleles for these SNPs is not possible, hence they are removed.

3) **Handle missing and nonsensical values**
   Some SNPs might have missing data, such that downstream analysis is not possible. Moreover, SNPs can have values which are not plausible such as negative standard errors or allele frequencies outside the span between 0 and 1. Additionally, at this step, all insertions and deletions (indels) are removed such that only biallelic SNPs remain.

4) **Filter SNPs on allele frequency and sample size**
   If the sample size is too low in combination with a low true minor allele frequency (MAF), the estimated MAF becomes unreliable. The filtering relies of minor allele counts (MAC) which is calculated as $\text{MAC} = 2 \cdot \text{N} \cdot \text{MAF}$, where N is the SNP sample size. All SNPs with $\text{MAC} \leq 6$ are removed.

5) **Remove data on sex chromosomes**
Sex chromosome SNPs adds complexity and might add biases to the analysis, autosomal SNPs thus provide cleaner, more reliable IVs for MR.

6) **Duplicates**
In case there are duplicated SNPs, keep only one instance.

### 3.3.1 Quality check: Identifying problems in the data

The final step aims to identify potential errors in the filtered data that may introduce bias in downstream analyses. Several diagnostic plots and summary statistics were used for this purpose.

1. **P-Z plot:** The P–Z plot compares reported p-values to p-values recalculated from Z-statistics as a consistency check.

$$Z = \beta / SE(\beta)$$
$$p = 2 \cdot (1 - \Phi(|Z|)),$$

where $\Phi$ denotes the cumulative distribution function of the standard normal distribution. Agreement between reported and recalculated p-values indicates internal consistency, while deviations may reflect errors in effect sizes or standard errors.

2. **Q-Q plot:** A quantile-quantile (Q-Q) plot compares the distribution of observed p-values to the expected distribution under the null hypothesis of no association.

The observed p-values are ordered as:

$$p_{(1)} \leq p_{(2)} \leq \cdots \leq p_{(n)},$$

where $i = 1, \ldots, n$ denotes the rank of the ordered p-values.

Under the null hypothesis, p-values follow a uniform distribution on $[0, 1]$, and the expected values are given by:

$$\mathbb{E}[p_{(i)}] = \frac{i}{n+1}.$$

The Q-Q plot is constructed by plotting:

$$-\log_{10}(p_{(i)}) \quad \text{vs.} \quad -\log_{10}\left(\frac{i}{n+1}\right).$$

Under the null hypothesis, the points lie along the identity line ($y = x$). Upward deviation from the line at its right tail indicates an excess of small p-values, which may reflect true associations or inflation due to confounding factors such as population stratification. Systematic deviation of the bulk of points from the line suggests inflation, whereas downward deviation indicates deflation.

3. $\boldsymbol{\lambda_{GC}}$: The genomic control inflation factor quantifies whether the distribution of test statistics deviates from the null expectation [21].

   Test statistics are obtained from p-values using the inverse cumulative distribution function of a chi-square distribution with one degree of freedom:

   $$\chi_i^2 = F_{\chi_1^2}^{-1}(1 - p_i).$$

   Under the null hypothesis, a $\chi^2$ distribution with one degree of freedom has median:

   $$\text{median}(\chi_1^2) \approx 0.455.$$

   The genomic control inflation factor is defined as:

   $$\lambda_{GC} = \frac{\text{median}(\chi^2_{\text{observed}})}{0.455}.$$

   Values of $\lambda_{GC} \approx 1$ indicate well-calibrated test statistics. Values $\lambda_{GC} > 1$ suggest inflation, which may arise from population stratification, while $\lambda_{GC} < 1$ indicates deflation, potentially due to overcorrection.

4. **EAF plot:** Observed effect allele frequencies (EAF) were compared against a reference panel to identify potential strand mismatches or allele misalignment.

   The Haplotype Reference Consortium (HRC) reference panel [22] was used, restricting to individuals of European ancestry to match the GWAS summary statistics. As the HRC data are provided in the hg19 genome build, coordinates were lifted to hg38 to ensure consistency with the GWAS data (see Section 3.3.2).

   Concordance between observed and reference allele frequencies is expected under correct alignment. Systematic deviations, such as mirroring around 0.5, may indicate strand inconsistencies or allele flipping.

### 3.3.2 Genome liftover

GWAS rely on reference genome builds for SNP coordinates. To ensure consistency when integrating datasets, all summary statistics must be aligned to the same genome build, as genomic coordinates may differ between builds.

Liftover was performed using the software *Score* [23], a toolkit for processing GWAS summary statistics. Score implements coordinate conversion by mapping variants between genome builds using reference genomes for the source and target builds, together with chain files that encode the alignment between assemblies.

Most datasets were provided in the hg38 genome build, which is the most recent and widely used assembly. Summary statistics not originally in hg38 were therefore lifted over to hg38 to ensure consistency across datasets.

## 3.4 Meta-analysis: Combining GWAS summary statistics datasets

When multiple GWAS were available for the same metabolite, summary statistics were combined using meta-analysis to increase statistical power and obtain more precise estimates of genetic associations. Meta-analysis was performed using the software METAL [24], which is widely used for the meta-analysis of GWAS summary statistics.

An inverse-variance weighted (IVW) method was applied, where the effect estimates from each study were weighted by the inverse of their squared standard errors. For a SNP $i$ in dataset $j$, the weight is calculated as

$$w_{i,j} = \frac{1}{SE_{i,j}^2},$$

where SE is the standard error for the effect estimate. For each SNP, the combined effect estimate was calculated as a weighted average of the study-specific effect sizes. The weighted effect estimate $\hat{\beta}_{IVW,i}$ for a SNP is then obtained by

$$\hat{\beta}_{IVW,i} = \frac{\sum_{j=1}^{n} w_{i,j}\hat{\beta}_i}{\sum_{j=1}^{n} w_{i,j}}.$$

The weighted standard error is then calculated as

$$SE_{IVW,i} = \sqrt{\frac{1}{\sum_{i=j}^{n} w_{i,j}}}.$$

This approach gives greater weight to studies with more precise estimates and assumes that all studies estimate the same underlying genetic effect.

## 3.5 Instrument variable selection

SNPs were filtered in according to the genome-wide p-value threshold of $5 \cdot 10^{-8}$, such that only statistically significant SNPs are passed to be selected as IVs.

### 3.5.1 Linkage disequilibrium pruning

According to the core assumptions of MR, the SNPs used as IVs should be independent of one another. Violations of this independence assumption can occur when SNPs are in linkage disequilibrium (LD), meaning that they are correlated due to non-random inheritance patterns within the genome. Including correlated variants as IVs can lead to biased causal effect estimates and inflated precision in MR analyses.

To ensure independence among selected IVs, linkage disequilibrium pruning was performed using PLINK2 [25]. SNPs were pruned based on pairwise LD, retaining only one variant from each set of correlated SNPs. Pruning was conducted using a sliding window approach, where within a defined genomic window, SNPs exceeding a specified LD threshold were removed. The variant with the strongest association with the exposure (i.e., the lowest p-value) was retained.

LD estimates were calculated using the 1000 Genomes phase 3 reference panel, selecting only for individuals with European ancestry to ensure accurate representation of LD structure [26]. Only SNPs passing the LD pruning criteria were retained for downstream MR analysis, thereby satisfying the independence assumption of the IVs.

## 3.6 Checking for weak instrumental variables

In MR analyses, an IV is considered weak if it explains only a small proportion of the variance in the exposure. Weak IVs can lead to biased causal effect estimates and inflated Type I error rates, particularly when there is overlap between the samples used to estimate the exposure and outcome associations.

IV strength was assessed using the F-statistic, which quantifies the strength of the association between the IV and the exposure. For an individual SNP, the F-statistic can be approximated as

$$F = \frac{\beta_X^2}{\mathrm{SE}_X^2},$$

where $\beta_X$ and $\mathrm{SE}_X$ denote the estimated effect size and standard error of the SNP–exposure association, respectively.

Following conventional guidelines, an F-statistic greater than 10 was taken to indicate sufficient IV strength, whereas an F-statistic of 10 or less was considered indicative of weak IVs [27].

## 3.7 Mendelian randomization analysis

Causal effect estimations were performed within a two-sample MR framework, namely the R package *TwoSampleMR*. Only SNPs that passed quality control, linkage disequilibrium pruning, and IV selection criteria were included in the analysis.

### 3.7.1 Causal effect estimation

The basis for causal effect estimation is the Wald ratio, defined for a SNP $i$ as:

$$\hat{\beta}_i = \frac{\hat{\beta}_{Yi}}{\hat{\beta}_{Xi}},$$

where $\hat{\beta}_{Yi}$ and $\hat{\beta}_{Xi}$ are the SNP–outcome and SNP–exposure associations, respectively.

For multiple IVs, the inverse-variance weighted (IVW) method combines the SNP-specific causal estimates into a single causal effect estimate:

$$\hat{\beta}_{IVW} = \frac{\sum_i w_i \hat{\beta}_i}{\sum_i w_i} = \frac{\sum_i \frac{\hat{\beta}_{Xi}\hat{\beta}_{Yi}}{SE^2_{Yi}}}{\sum_i \frac{\hat{\beta}^2_{Xi}}{SE^2_{Yi}}},$$

where the weights are defined as $w_i = 1/SE^2_{Yi}$, corresponding to the inverse variance of the SNP–outcome association.

The primary causal effect estimates for each metabolite were obtained using the IVW method. This approach combines the Wald ratios across all IVs into a single overall causal estimate, weighting each SNP by the inverse of the variance of its outcome association.

#### 3.7.1.1 Horizontal pleiotropy and heterogeneity tests

Heterogeneity among SNP-specific causal effect estimates was assessed using Cochran's $Q$ statistic. For $K$ IVs, the statistic is defined as:

$$Q = \sum_{i=1}^{K} w_i(\hat{\beta}_i - \hat{\beta}_{\mathrm{IVW}})^2,$$

where $\hat{\beta}_i$ is the causal effect estimate for SNP $i$, $\hat{\beta}_{\mathrm{IVW}}$ is the IVW causal effect estimate, and $w_i$ are the inverse-variance weights [28]. Under the null hypothesis of

homogeneity, $Q$ follows a $\chi^2$ distribution with $K-1$ degrees of freedom. A significant $Q$ statistic indicates heterogeneity across SNP-specific causal effect estimates, which may reflect violations of IV assumptions.

Directional horizontal pleiotropy was evaluated using the MR-Egger intercept test [29]. In this framework, the SNP-outcome associations are regressed on the SNP-exposure associations:

$$\hat{\beta}_{Y,i} = \alpha + \beta_{\text{Egger}}\hat{\beta}_{X,i} + \epsilon_i,$$

where $\alpha$ represents the intercept. A statistically significant non-zero intercept ($\alpha \neq 0$) provides evidence of directional horizontal pleiotropy, indicating that SNPs may influence the outcome through pathways independent of the exposure.

## 3.8 Code availability

All analyses were built into a pipeline using the workflow manager Snakemake. The scripts used to perform data harmonization, causal effect estimation, and sensitivity analyses are available at https://github.com/oerp0315/psc-metabolite-causality.

# 4

# Results

This section presents the results of the MR analysis investigating the causal effects of blood circulating metabolites on the risk of PSC. First, an overview of the GWAS datasets included in the study is provided, followed by an example from the quality check of quality controlled GWAS summary statistic data. Next, the results of IV selection are reported, followed by the MR analysis estimating causal effects. Results are reported for both individual GWAS datasets and meta-analysed datasets where multiple studies were available for a given metabolite. Sensitivity analyses and tests for pleiotropy and heterogeneity are then presented.

## 4.1 Study and data overview

An overview of the GWAS included in the analyses is provided below. This includes information on the metabolite GWAS datasets used as exposures and the PSC GWAS datasets used as outcomes, along with key characteristics such as sample size, number of associated SNPs found and genomic build used.

### 4.1.1 Metabolite GWAS datasets

An overview of the metabolite GWAS datasets included as exposures in this study is presented in Table 4.1. The table summarizes key characteristics of each dataset, including sample size, number of reported associated SNPs, and genomic build, which are relevant for downstream quality control and IV selection. All datasets presented in this table were obtained from GWAS catalog [30], and can be found using the ID column values.

### 4.1.2 PSC GWAS datasets

GWAS datasets included for PSC in this study are summarized in Table 4.2. The dataset with ID GCST004030 was obtained from GWAS catalog [30], whereas the dataset finngen_R12_K11_PSC_COLITIS_STRICT was obtained from the FinnGen consortium [31, 32].

**Table 4.1:** Genome-wide association studies of metabolites used as exposure datasets in the MR analysis, including sample size and number of associated SNPs found. All datasets collected for PSC-associated and non-associated metabolites were already in genome build hg38, hence no liftover was performed.

| Metabolite | ID | Sample Size | Assoc. SNPs |
|---|---|---|---|
| **PSC-associated metabolites** | | | |
| Imidazole propionate | GCST90199915 | 7776 | 1 |
| | GCST90615799 | 2392 | 0 |
| 3-methyl-2-oxovalerate | GCST90199631 | 8257 | 0 |
| | GCST90615407 | 2392 | 0 |
| 4-methyl-2-oxopentanoate | GCST90199655 | 8255 | 0 |
| | GCST90615432 | 2392 | 0 |
| Oxalate | GCST90199672 | 8181 | 1 |
| | GCST90615459 | 2392 | 0 |
| Threonate | GCST90199687 | 8151 | 1 |
| | GCST90615476 | 2392 | 0 |
| Pimeloylcarnitine | GCST90200101 | 7837 | 5 |
| | GCST90616070 | 2392 | 1 |
| **Non-associated metabolites** | | | |
| Phenylacetate | GCST90199630 | 7059 | 1 |
| | GCST90615403 | 2392 | 1 |
| Citrulline | GCST90200403 | 8157 | 2 |
| | GCST90616468 | 2392 | 0 |
| Maltose | GCST90200447 | 6351 | 0 |
| | GCST90616526 | 2392 | 0 |
| Arabinose | GCST90616516 | 2392 | 0 |
| Succinoyltaurine | GCST90616288 | 2392 | 1 |
| Octanoylcarnitine (C8) | GCST90199720 | 8226 | 4 |
| | GCST90615518 | 2392 | 1 |
| Phenyllactate (PLA) | GCST90199664 | 8235 | 1 |
| | GCST90615449 | 2392 | 1 |

**Table 4.2:** Genome-wide association studies of PSC used as outcome datasets in the MR analysis, including sample size, number of associated SNPs found and genome build used.

| Metabolite | ID | Sample Size | Assoc. SNPs | Build |
|---|---|---|---|---|
| PSC | GCST004030 | 14890 | 30 | hg38 |
| | finngen_R12_K11_ PSC_COLITIS_ STRICT | 498415 | Not reported | hg19 |

## 4.2 Quality control

Quality control was performed on all collected datasets, plots visualizing the data after quality control can be found in Appendix A. Here quality plots from imidazole propionate, one of the metabolites associated to PSC, is presented. It is clear that the GWAS found a region of significant SNPs on chromosome 12 (Fig. 4.1a). Furthermore, the general pattern of allele frequencies matches that of the reference panel, indicated by the points following the red trend line 4.1b. However, points deviating from the trend line are present in an inversed N-like shape, a pattern that is consistent over all datasets (Appendix A). The QQ-plot show a rapid increase from the trend line at high $-\log_{10}(\text{p})$ values, indicating that there is a higher abundance of low p-values than would be expected under the assumption that no significant SNPs are present (4.1c). This observation is further reinforced by the $\lambda_{GC} = 1.011$, which is close to 1, implying that the number of significant SNPs found is neither underinflated nor inflated. All points in the P-Z plot are located on the trend line, indicating that effect estimates, standard errors and p-values all match within each SNP (4.1d).

## 4.3 Instrumental variable selection

This section summarizes the IV selection process of the IVs used in the MR analysis. For each metabolite, the number of genome-wide significant variants identified, the number of variants retained after linkage disequilibrium pruning, and the final number of IVs used for analysis are reported. IV strength was assessed using F-statistics, which are summarized by minimum, maximum, and mean values to evaluate the potential risk of weak IV bias.

### 4.3.1 Instrumental variable selection steps

For metabolites with GWAS summary statistics available from multiple studies, meta-analysis was performed prior to IV selection. Metabolites with only one available

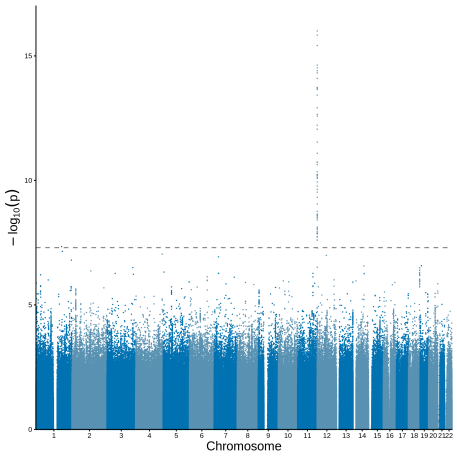


**(a)** Manhattan plot showing genome-wide significance of SNPs. The dashed line represent a genome-wide significance threshold of $5 \times 10^{-8}$. A spike appears above the threshold line in chromosome 12, indicating a group of SNPs having a signifcant effect on imidazole propionate.

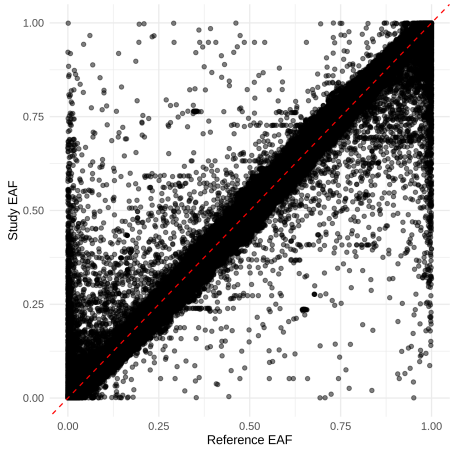


**(b)** Effect allele frequency plot comparing allele frequencies between the HRC reference panel and the GWAS study. The majority of the SNPs fall on the identity line, with some deviating SNPs forming an inverse N-shape.

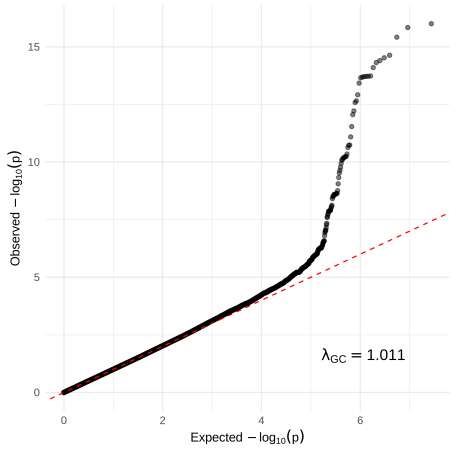


**(c)** QQ-plot comparing p-values in the GWAS summary to an uniform distribution of p-values. Points on the red dashed line follow this uniform distribution. A rise over the identity line at high -$\log_{10}$(p) indicates the existence of more SNPs with a low p-values than would be expected by pure chance.

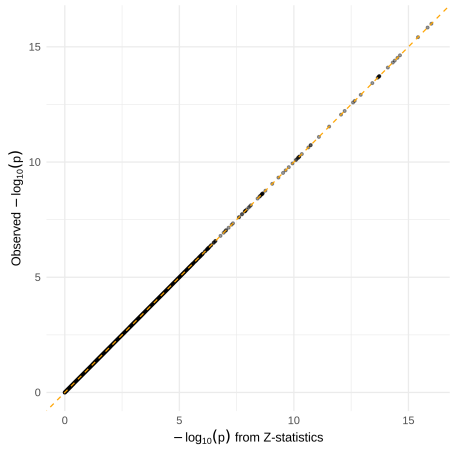


**(d)** P-Z plot comparing the observed p-values to p-values calculated from Z-statistics. SNPs fall without deviation on the identity line, showing that effect estimates, standard errors and p-values are consistent with each other, within each SNP.

**Figure 4.1:** Data visualisation of imidazole propionate (GCST90199915) GWAS summary statistics after quality control.

GWAS summary statistics datasets, the dataset was kept as is for the IV selection. Table 4.3 summarizes the number of genome-wide significant SNPs identified in the meta-analysed datasets, along with the number of variants retained after LD pruning and the final number of IVs used in the MR analysis.

Across meta-analysed metabolites, the number of IVs ranged from 0 to 5, with three metabolites (3-methyl-2-oxovalerate and maltose) with no found IVs (Table 4.3). Hence, these metabolites could not be included in the remaining part of the causal effect estimation. For both threonate and phenylacetate, SNP was discarded from the LD clumped SNPs since that SNP was not present in the PSC GWAS dataset.

**Table 4.3:** Genome-wide significant SNPs for each metabolite are clumped together with respect to linkage disequilibrium. The final step for IV selection is to remove SNPs that are not present in the PSC GWAS dataset.

| Metabolite | Sign. SNPs | Clumped SNPs | No. IVs |
|---|---|---|---|
| **PSC-associated metabolites** | | | |
| Imidazole propionate | 30 | 1 | 1 |
| 3-methyl-2-oxovalerate | 0 | 0 | 0 |
| 4-methyl-2-oxopentanoate | 0 | 0 | 0 |
| Oxalate | 1 | 1 | 1 |
| Threonate | 3 | 2 | 1 |
| Pimeloylcarnitine | 279 | 5 | 5 |
| **Non-associated metabolites** | | | |
| Phenylacetate | 73 | 3 | 2 |
| Citrulline | 8 | 2 | 2 |
| Maltose | 0 | 0 | 0 |
| Arabinose | 5 | 4 | 4 |
| Succinoyltaurine | 221 | 2 | 2 |
| Octanoylcarnitine | 896 | 5 | 5 |
| Phenyllactate | 304 | 2 | 2 |

### 4.3.2 Checking for weak instrumental variables

IV strength was assessed using the F-statistic for each IV. The calculated F-statistics were all below the conventional threshold of 10, ranging from 0.009 to 4.952 (Table 4.4).

These results indicate that the selected IVs are weak IVs for the metabolite exposures, explaining only a limited proportion of the variance in the phenotype. The presence

of weak IVs may reduce the reliability of MR causal effect estimates and increase susceptibility to bias.

**Table 4.4:** Overview of F-values for IVs in both PSC-associated and non-associated metabolites in the meta-analysed . For each metabolites, the total number of IVs as well as the mean, minimum value and maximum value is reported.

| Metabolite | No. IVs | Mean F | Min F | Max F |
|---|---|---|---|---|
| **PSC-associated metabolites** | | | | |
| Imidazole propionate | 1 | 3.017 | 3.017 | 3.017 |
| Oxalate | 1 | 0.325 | 0.325 | 0.325 |
| Threonate | 1 | 1.903 | 1.903 | 1.903 |
| Pimeloylcarnitine | 5 | 1.563 | 0.303 | 4.835 |
| **Non-associated metabolites** | | | | |
| Arabinose | 4 | 2.105 | 0.276 | 4.952 |
| Succinoyltaurine | 2 | 1.053 | 0.032 | 2.074 |
| Octanoylcarnitine | 5 | 1.020 | 0.009 | 2.773 |
| Phenylacetate | 2 | 0.509 | 0.064 | 0.953 |
| Citrulline | 2 | 0.017 | 0.009 | 0.026 |
| Phenyllactate | 2 | 0.997 | 0.012 | 1.983 |

## 4.4 Mendelian Randomization

### 4.4.1 Causal effect estimates

In Fig. 4.2, causal effect estimates for the PSC-associated metabolites are shown, calculated either through the Wald ratio for metabolites with only one IV or IVW for those with more than one IV. At a 95% confidence interval all metabolites overlap with 0, indicating no causal effect. Detailed causal effect estimates for each IVs per metabolite are available in Appendix C.

A similar pattern is present for the non-associated metabolites, with all metabolites overlapping with 0 (Fig. 4.3). Citrulline show a significantly larger uncertainty in the causal effect estimate, but with a mean that falls very close to 0. The non-associated metabolites altogether show no causal effect on PSC.

### 4.4.2 Sensitivity analysis

Only pimeloylcarnitine yielded a Cochran's Q statistic among the PSC-associated metabolites, as two or more IVs are necessary to evaluate heterogeneity among the instruments (Table 4.5). For pimeloylcarnitine, some heterogeneity is present, as

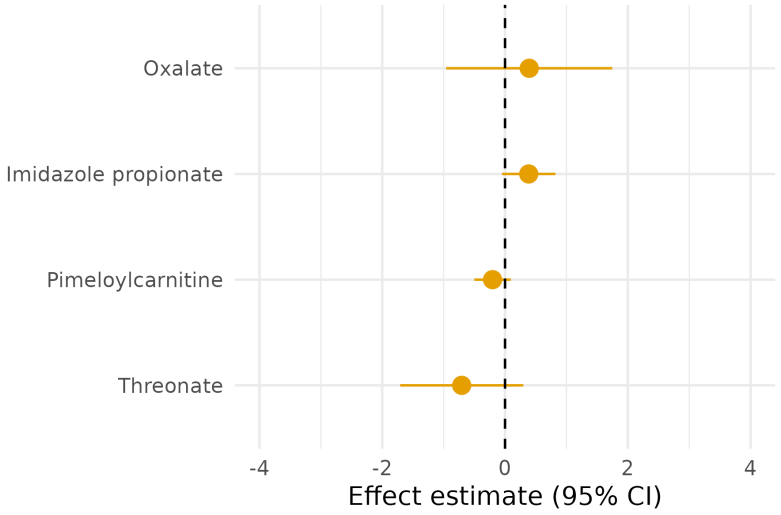


**Figure 4.2:** The causal effect estimates for the PSC-associated metabolites fall close to 0, with a confidence interval of 95% overlapping with 0 for all metabolites.

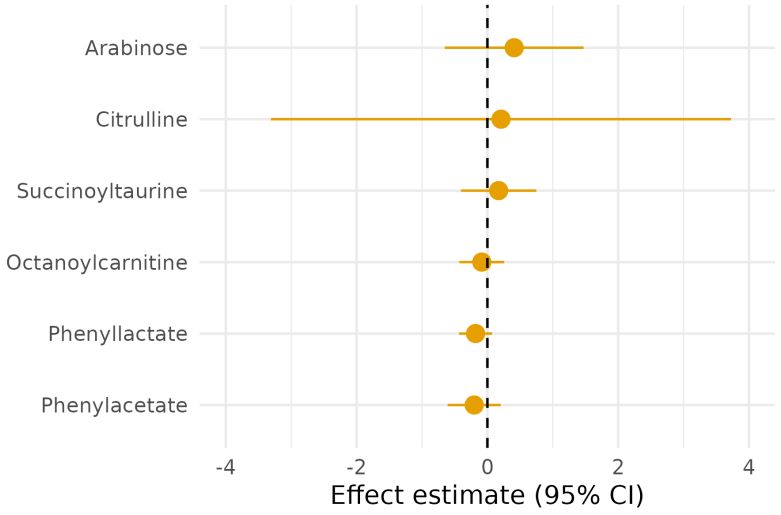


**Figure 4.3:** The causal effect estimates for the non-associated metabolites fall close to 0, with a confidence interval of 95% overlapping with 0 for all metabolites.

the Cochran's Q statistic is relatively high compared to the degrees of freedom, indicating some deviation in the causal effect estimates for the individual IVs.

Among the non-associated metabolites, a similar pattern is observed for arabinose, succinoyltaurine, and octanoylcarnitine. In contrast, phenylacetate, citrulline, and phenyllactate show very low heterogeneity.

**Table 4.5:** Heterogeneity between causal effect estimates from each IV per metabolites is tested. If cochran's Q » degree of freedom, there is heterogeneity between IVs.

| Metabolite | No. IVs | Cochran's Q | Degrees of freedom |
|---|---|---|---|
| **PSC-associated metabolites** | | | |
| Pimeloylcarnitine | 5 | 5.34 | 4 |
| **Non-associated metabolites** | | | |
| Arabinose | 4 | 7.1 | 3 |
| Succinoyltaurine | 2 | 1.6 | 1 |
| Octanoylcarnitine | 5 | 4.8 | 4 |
| Phenylacetate | 2 | 0.07 | 1 |
| Citrulline | 2 | 0.02 | 1 |
| Phenyllactate | 2 | 0.02 | 1 |

For each of the metabolites with more than 3 IVs, MR-egger regression could be performed to check for horizontal pleiotropy. This is the case for pimeloylcarnitine from the PSC-associated metabolites and arabinose and octanoylcarnitine from the non-associated metabolites. Figure 4.4 show a scatter plot for pimeolycarnitine with MR-egger regression in dark blue and the IVW regression in light blue. The IVW regression is confined to the origin by definition whereas MR-egger deviates slightly from the origin, indicating a small but negligible horizontal pleiotropic effect. Corresponding plot for arabinose and octanoylcarnitine are found in Appendix C.

## 4.5 MR causal effect comparison to Molinaro et al. effect estimates

Comparable effect sizes was provided by Molinaro et al. (Table 4.6) which are in this section compared to the causal effect estimates obtained in this study.

MR causal effect estimates for all PSC-associated metabolites except for oxalate have the same sign compared to the effect sizes obtained by Molinaro et al., showing some similarity to those results. These metabolites show a more conservative causal effect

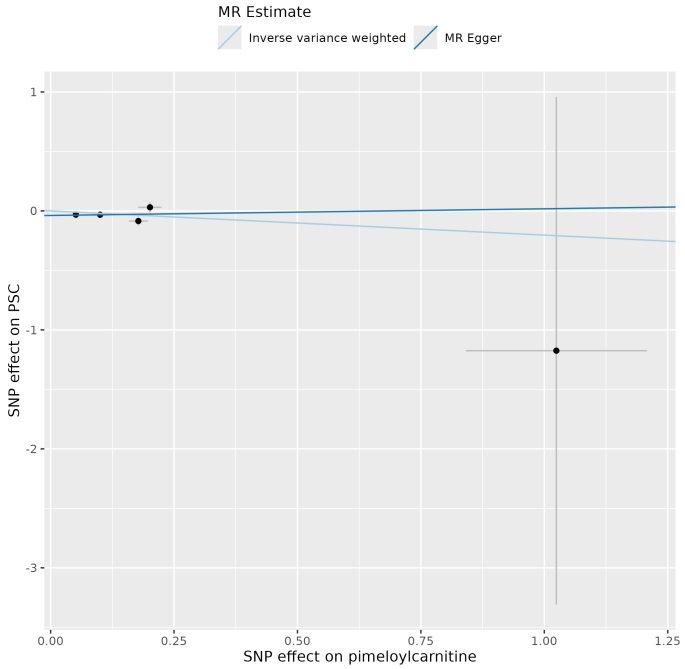


**Figure 4.4:** Scatter plot where each dot represents an IV, dark and light blue lines represent MR-Egger and IWV regression respectively.

**Table 4.6:** Effect estimates from Molinaro et al. for both PSC-associated and non-associated metabolites with corresponding standard errors. Oxalate deviates most from the Molinaro et al. effect estimates, showing a slightly positive effect. The other metabolites show more similar results, though a conservative with causal effect estimates closer to 0.

| Metabolite | Effect estimate | Standard error |
|---|---|---|
| **PSC-associated metabolites** | | |
| Imidazole propionate | 0.88 | 0.25 |
| Oxalate | -2.53 | 0.71 |
| Threonate | -1.61 | 0.48 |
| Pimeloylcarnitine | -0.84 | 0.27 |
| **Non-associated metabolites** | | |
| Arabinose | -0.02 | 0.42 |
| Succinoyltaurine | 0.04 | 0.26 |
| Octanoylcarnitine | 0.04 | 0.24 |
| Phenylacetate | 0.02 | 0.20 |
| Citrulline | 0.05 | 0.49 |
| Phenyllactate | 0.02 | 0.38 |

estimate comparing to the results of Molinaro et al., forming an apparent trend line, thought with a steeper slope.

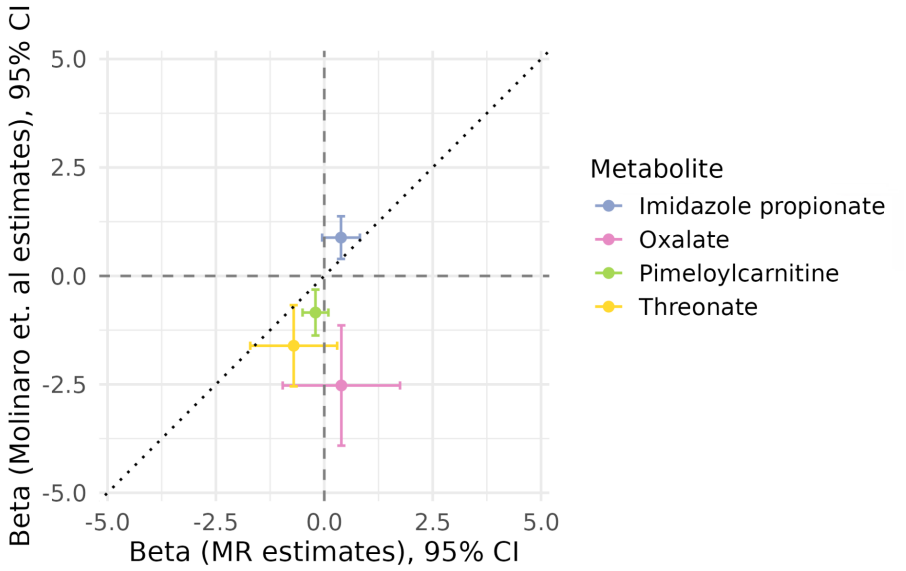


**Figure 4.5:** Comparison of effect estimates provided by Molinaro et al. and causal effect estimates obtained through MR for PSC-associated metabolites. The closer metabolites are to the trend line, the more similar the causal effect estimate from MR is to the effect estimates from Molinaro et al.

The non-associated metabolites show a very clear pattern, in which the causal effect estimates closely grouped near 0, supporting the results for the non-associated metabolism of Molinaro et al. (Fig 4.6).

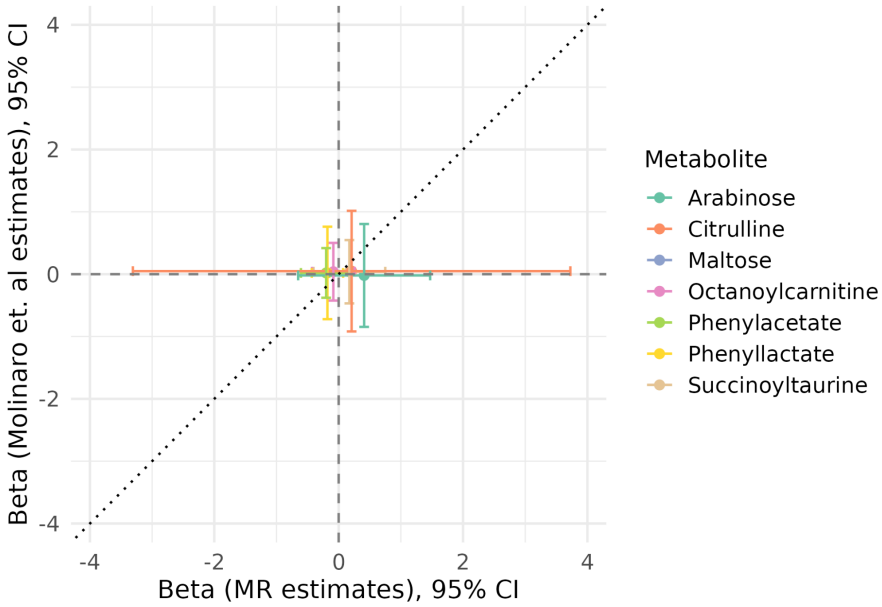


**Figure 4.6:** Comparison of effect estimates provided by Molinaro et al. and causal effect estimates obtained through MR for metabolites not associated with PSC. The closer metabolites are to the trend line, the more similar the causal effect estimate from MR is to the effect estimates from Molinaro et al.

# 5

# Discussion

The aim of this study was to investigate potential causal effects of blood circulating metabolites on the risk of PSC using a two-sample MR framework. Overall, no evidence of a causal effect was identified for either the metabolites previously associated with PSC or the selected non-associated metabolites. All estimated causal effects were close to zero, with confidence intervals overlapping the null, indicating a lack of statistically significant associations.

Despite the absence of detectable causal effects, the results showed partial consistency with previous observational findings. For several metabolites previously reported to be associated with PSC, the direction of the estimated causal effects was consistent with those reported by Molinaro et al., although the magnitude of the effects was substantially smaller and not statistically significant. This pattern suggests that while observational associations may reflect underlying biological relationships, they may not represent causal effects. Alternatively, true causal effects may exist but be too small to detect given the limited statistical power of the present analysis.

A key limitation of this study is the weak strength of the instrumental variables. The F-statistics for all instruments were below the conventional threshold of 10, indicating that the selected IVs explain only a small proportion of the variance in metabolite levels. Weak instruments are known to bias MR causal effect estimates towards the null and reduce statistical power, making it difficult to detect true causal effects. Consequently, the absence of significant findings in this study should be interpreted with caution, as it may reflect insufficient instrument strength rather than a true lack of causal relationships.

In addition, the number of available instrumental variables was limited for several metabolites, in some cases consisting of only a single SNP. This restricts the application of sensitivity analysis and reduces the robustness of the causal estimates. Methods such as MR-Egger and heterogeneity tests rely on multiple independent instruments to provide reliable assessments of pleiotropy and consistency across SNP-specific effects. The limited number of instruments therefore constrains the ability to fully evaluate violations of the MR assumptions.

Some degree of heterogeneity was observed among SNP-specific causal effect estimates for certain metabolites, suggesting variability in the estimated causal effects across

instruments. While there was little evidence of directional horizontal pleiotropy, as indicated by MR-Egger intercept tests, the presence of heterogeneity may reflect measurement error or pleiotropic effects. This highlights the complexity of using IVs for metabolite traits, which are often influenced by multiple biological pathways.

The inclusion of non-associated metabolites as negative controls provides additional support for the validity of the analytical framework. The observed clustering of causal effect estimates around zero for these metabolites is consistent with expectations and suggests that the analysis does not systematically produce false positive results. This strengthens confidence that the null findings for PSC-associated metabolites are not driven by methodological artifacts.

Taken together, the results suggest that the currently available IVs for the circulating metabolites are insufficient to robustly assess causal effects on PSC risk. The combination of weak instruments, limited SNP availability, and modest sample sizes in metabolite GWAS reduces the ability to draw definitive conclusions regarding causality.

More broadly, these findings highlight important considerations regarding the use of MR as a tool for causal inference. In recent years, MR has become increasingly accessible due to the availability of large-scale GWAS summary statistics and user-friendly software packages. While this has enabled rapid growth in MR studies, it also increases the risk of misinterpretation when analyses are conducted without careful evaluation of underlying assumptions.

In particular, issues such as weak instrument bias, horizontal pleiotropy, and sample overlap can substantially affect the validity of causal effect estimates. If these factors are not adequately addressed, MR analysis may yield biased or misleading results, including false negative findings or spurious evidence of causality. The present study illustrates how weak instrument strength can limit the ability to detect causal effects, even when observational associations exist.

Therefore, while MR represents a powerful framework for strengthening causal inference, its results should be interpreted in the context of instrument strength, robustness checks, and biological plausibility. Careful study design and critical evaluation of assumptions remain essential to avoid overinterpretation of findings.

Future studies would benefit from larger and more comprehensive metabolite GWAS, which could provide stronger and more reliable IVs. Improved instrument strength would increase the power of MR analysis and enable more definitive conclusions regarding the causal role of metabolites in PSC. In addition, the use of alternative approaches, such as multivariable MR, or integration with other omics data (e.g.,

transcriptomics or proteomics), may provide further insight into the biological mechanisms underlying PSC.

## 5.1 Conclusion

In this study, MR was applied to investigate potential causal effects of blood circulating metabolites on the risk of PSC. No evidence of causal effects was identified for either PSC-associated or non-associated metabolites.

However, the analysis was limited by weak instrument strength and a small number of available IVs, which reduces confidence in the null findings. The results therefore highlight important limitations in applying MR to metabolite data, rather than definitively excluding a causal role of these metabolites in PSC.

Overall, this study underscores the need for larger and more powerful metabolite GWAS to enable reliable causal inference, and demonstrates both the potential and the current limitations of MR in studying complex metabolic contributions to disease.

# Bibliography


1. Rawla P and Samant H. Primary Sclerosing Cholangitis. *StatPearls [Internet]*. [Updated 2023 Feb 12; cited 2025 Jan-]. Treasure Island (FL): StatPearls Publishing, 2025. Available from: `https://www.ncbi.nlm.nih.gov/books/NBK537181/`
2. Molinaro et al. Unpublished data on blood metabolites associated to PSC. 2026
3. Nguyen K and Mitchell BD. A guide to Understanding Mendelian randomization studies. Arthritis care & research 2024; 76:1451
4. Strazzabosco M and Fabris L. Functional anatomy of normal bile ducts. The Anatomical Record: Advances in Integrative Anatomy and Evolutionary Biology: Advances in Integrative Anatomy and Evolutionary Biology 2008; 291:653–60
5. Bjøro K, Brandsæter B, Foss A, and Schrumpf E. Liver transplantation in primary sclerosing cholangitis. *Seminars in liver disease*. Vol. 26. 01. Copyright© 2006 by Thieme Medical Publishers, Inc., 333 Seventh Avenue, New ... 2006 :69–79
6. Rabiee A and Silveira MG. Primary sclerosing cholangitis. Translational gastroenterology and hepatology 2021; 6:29
7. Manns MP, Bergquist A, Karlsen TH, Levy C, Muir AJ, Ponsioen C, Trauner M, Wong G, and Younossi ZM. Primary sclerosing cholangitis. Nature Reviews Disease Primers 2025; 11:17
8. Sheehan NA, Didelez V, Burton PR, and Tobin MD. Mendelian randomisation and causal inference in observational epidemiology. PLoS medicine 2008; 5:e177
9. Banack HR, Bea JW, Kaufman JS, Stokes A, Kroenke CH, Stefanick ML, Beresford SA, Bird CE, Garcia L, Wallace R, et al. The effects of reverse causality and selective attrition on the relationship between body mass index and mortality in postmenopausal women. American journal of epidemiology 2019; 188:1838–48
10. Uffelmann E, Huang QQ, Munung NS, De Vries J, Okada Y, Martin AR, Martin HC, Lappalainen T, and Posthuma D. Genome-wide association studies. Nature reviews methods primers 2021; 1:59
11. Hartwig FP, Davies NM, Hemani G, and Davey Smith G. Two-sample Mendelian randomization: avoiding the downsides of a powerful, widely applicable but potentially fallible technique. 2016
12. Carter AR and Anderson EL. Correct illustration of assumptions in Mendelian randomization. International Journal of Epidemiology 2024; 53:dyae050

13. Risch N and Merikangas K. The future of genetic studies of complex human diseases. Science 1996; 273:1516–7
14. Hayes B. Overview of statistical methods for genome-wide association studies (GWAS). Genome-wide association studies and genomic prediction 2013 :149–69
15. Bergquist A, Lindberg G, Saarinen S, and Broomé U. Increased prevalence of primary sclerosing cholangitis among first-degree relatives. Journal of hepatology 2005; 42:252–6
16. Ji SG, Juran BD, Mucha S, Folseraas T, Jostins L, Melum E, Kumasaka N, Atkinson EJ, Schlicht EM, Liu JZ, et al. Genome-wide association study of primary sclerosing cholangitis identifies new risk loci and quantifies the genetic relationship with inflammatory bowel disease. Nature genetics 2017; 49:269–73
17. Jiang X and Karlsen TH. Genetics of primary sclerosing cholangitis and pathophysiological implications. Nature reviews Gastroenterology & hepatology 2017; 14:279–95
18. Manolio TA, Collins FS, Cox NJ, Goldstein DB, Hindorff LA, Hunter DJ, McCarthy MI, Ramos EM, Cardon LR, Chakravarti A, et al. Finding the missing heritability of complex diseases. Nature 2009; 461:747–53
19. Davey Smith G and Hemani G. Mendelian randomization: genetic anchors for causal inference in epidemiological studies. Human molecular genetics 2014; 23:R89–R98
20. Winkler TW, Day FR, Croteau-Chonka DC, Wood AR, Locke AE, Mägi R, Ferreira T, Fall T, Graff M, Justice AE, et al. Quality control and conduct of genome-wide association meta-analyses. Nature protocols 2014; 9:1192–212
21. Devlin B and Roeder K. Genomic control for association studies. Biometrics 1999; 55:997–1004
22. A reference panel of 64,976 haplotypes for genotype imputation. Nature genetics 2016; 48:1279–83
23. Genovese G, Rockweiler NB, Gorman BR, Bigdeli TB, Pato MT, Pato CN, Ichihara K, and McCarroll SA. BCFtools/liftover: an accurate and comprehensive tool to convert genetic variants across genome assemblies. Bioinformatics 2024; 40:btae038
24. Willer CJ, Li Y, and Abecasis GR. METAL: fast and efficient meta-analysis of genomewide association scans. Bioinformatics 2010; 26:2190–1
25. Chang CC, Chow CC, Tellier LC, Vattikuti S, Purcell SM, and Lee JJ. Second-generation PLINK: rising to the challenge of larger and richer datasets. Gigascience 2015; 4:s13742–015
26. Byrska-Bishop M, Evani US, Zhao X, Basile AO, Abel HJ, Regier AA, Corvelo A, Clarke WE, Musunuri R, Nagulapalli K, et al. High-coverage whole-genome

sequencing of the expanded 1000 Genomes Project cohort including 602 trios. Cell 2022; 185:3426–40

27. Staiger DO and Stock JH. Instrumental variables regression with weak instruments. 1994
28. Bowden J, Del Greco M F, Minelli C, Zhao Q, Lawlor DA, Sheehan NA, Thompson J, and Davey Smith G. Improving the accuracy of two-sample summary-data Mendelian randomization: moving beyond the NOME assumption. International journal of epidemiology 2019; 48:728–42
29. Bowden J, Davey Smith G, and Burgess S. Mendelian randomization with invalid instruments: effect estimation and bias detection through Egger regression. International journal of epidemiology 2015; 44:512–25
30. Buniello A, MacArthur JAL, Cerezo M, Harris LW, Hayhurst J, Malangone C, McMahon A, Morales J, Mountjoy E, Sollis E, et al. The NHGRI-EBI GWAS Catalog of published genome-wide association studies, targeted arrays and summary statistics 2019. Nucleic acids research 2019; 47:D1005–D1012
31. Kurki MI, Karjalainen J, Palta P, Sipilä TP, Kristiansson K, Donner KM, Reeve MP, Laivuori H, Aavikko M, Kaunisto MA, et al. FinnGen provides genetic insights from a well-phenotyped isolated population. Nature 2023; 613:508–18
32. FinnGen. FinnGen Documentation of R12 release. 2024. Available from: `https://finngen.gitbook.io/documentation/` [Accessed on: 2026 Apr 22]

# A

# Quality control plots

## A.1 PSC-associated metabolites

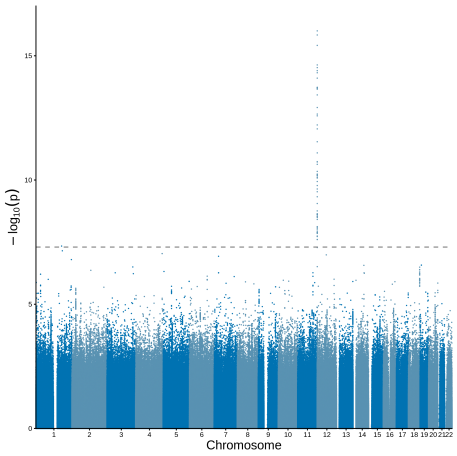


**(a)** Manhattan plot for imidazole propionate (GCST90199915)

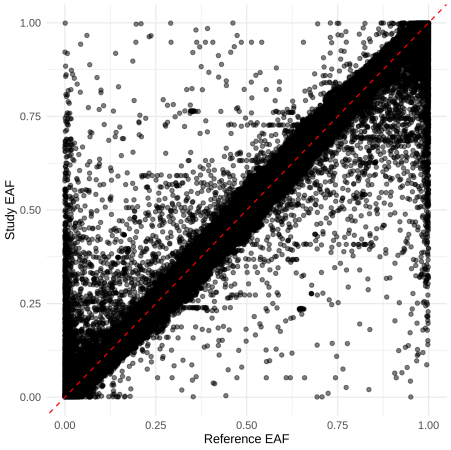


**(b)** EAF plot for imidazole propionate (GCST90199915)

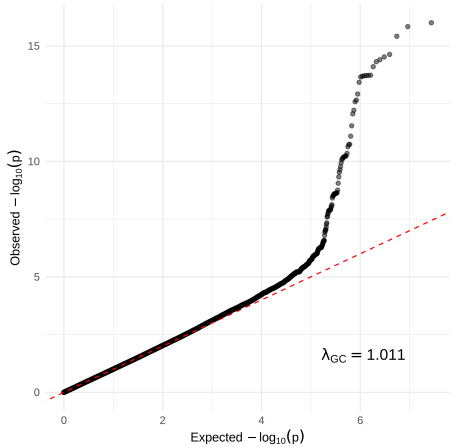


**(c)** Q-Q plot for imidazole propionate (GCST90199915)

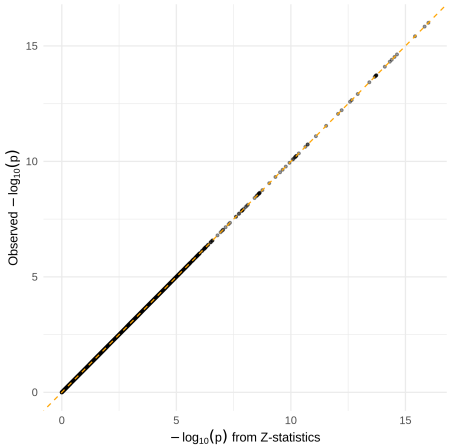


**(d)** P-Z plot for imidazole propionate (GCST90199915)

**Figure A.1:** Quality control plots for the GWAS dataset of imidazole propionate (GCST90199915), including Manhattan, effect allele frequency (EAF), Q-Q, and P-Z plot.

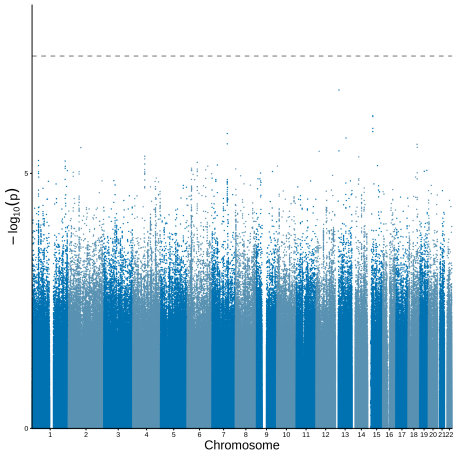


**(a)** Manhattan plot for imidazole propionate (GCST90615799)

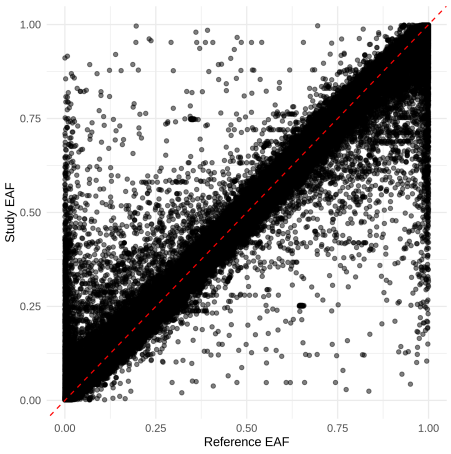


**(b)** EAF plot for imidazole propionate (GCST90615799)

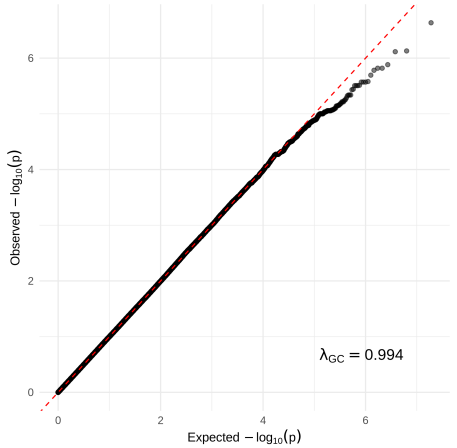


**(c)** Q-Q plot for imidazole propionate (GCST90615799)

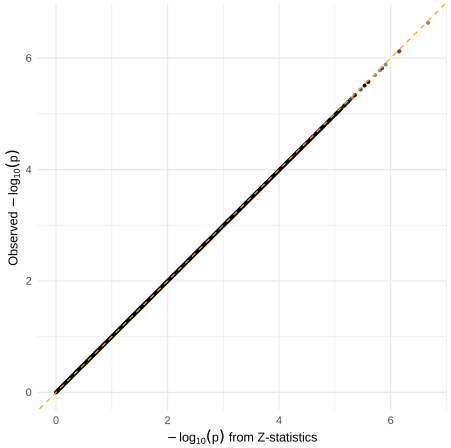


**(d)** P-Z plot for imidazole propionate (GCST90615799)

**Figure A.2:** Quality control plots for the GWAS dataset of imidazole propionate (GCST90615799), including Manhattan, effect allele frequency (EAF), Q-Q, and P-Z plot.

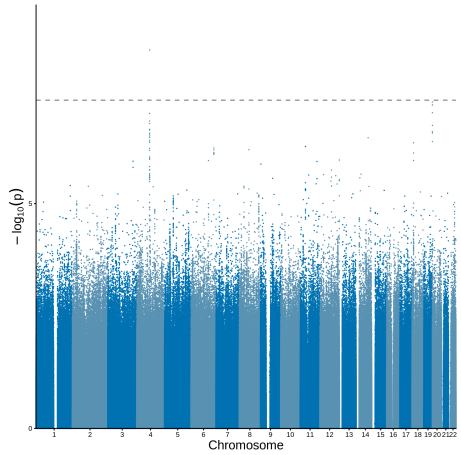


**(a)** Manhattan plot for 3-methyl-2-oxovalerate (GCST90199631)

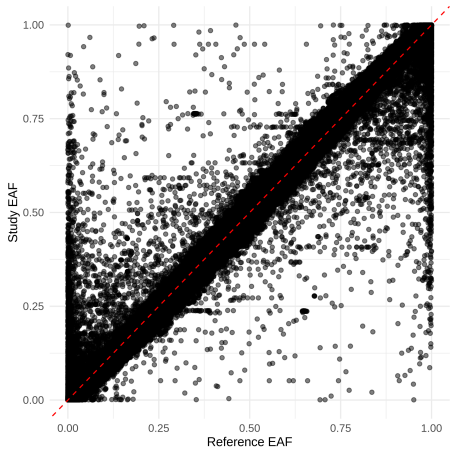


**(b)** EAF plot for 3-methyl-2-oxovalerate (GCST90199631)

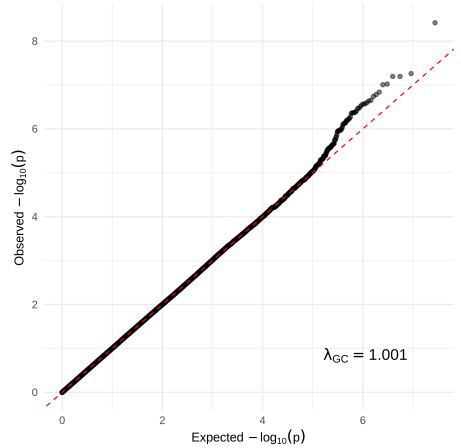


**(c)** Q-Q plot for 3-methyl-2-oxovalerate (GCST90199631)

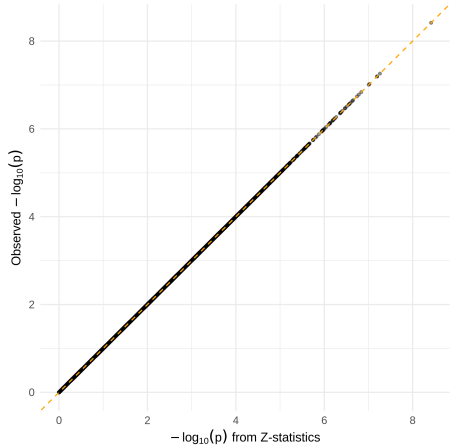


**(d)** P-Z plot for 3-methyl-2-oxovalerate (GCST90199631)

**Figure A.3:** Quality control plots for the GWAS dataset of 3-methyl-2-oxovalerate (GCST90199631), including Manhattan, effect allele frequency (EAF), Q-Q, and P-Z plot.

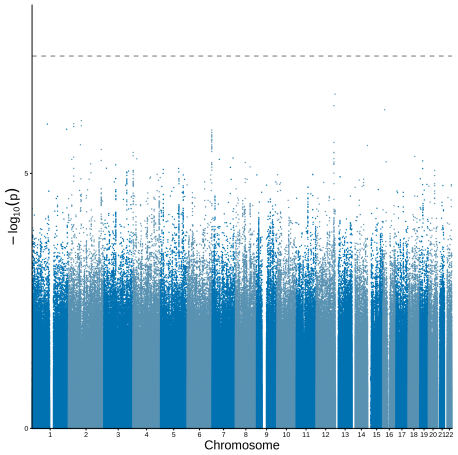


**(a)** Manhattan plot for 3-methyl-2-oxovalerate (GCST90615407)

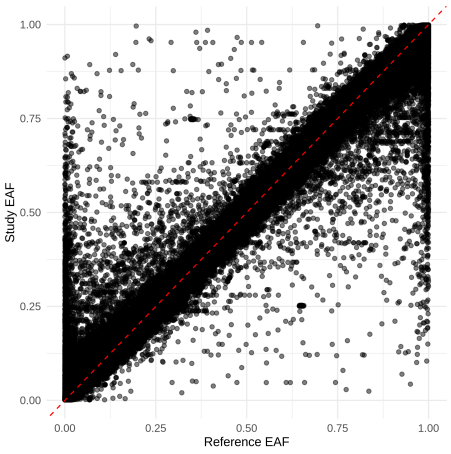


**(b)** EAF plot for 3-methyl-2-oxovalerate (GCST90615407)

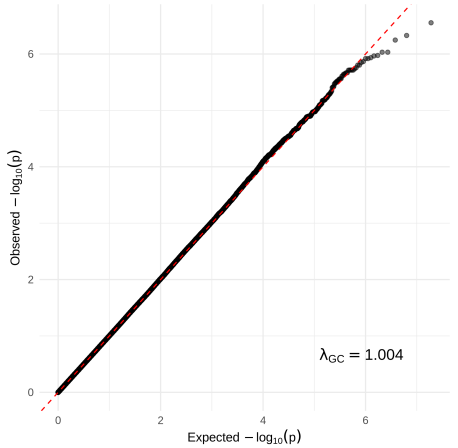


**(c)** Q-Q plot for 3-methyl-2-oxovalerate (GCST90615407)

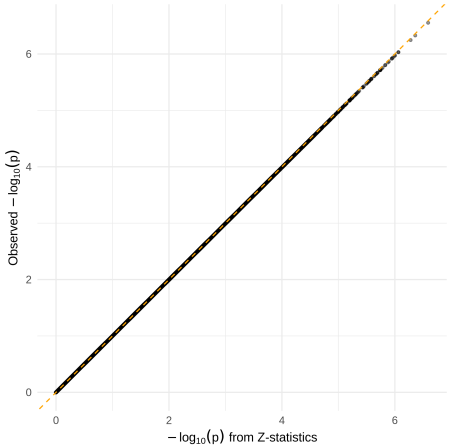


**(d)** P-Z plot for 3-methyl-2-oxovalerate (GCST90615407)

**Figure A.4:** Quality control plots for the GWAS dataset of 3-methyl-2-oxovalerate (GCST90615407), including Manhattan, effect allele frequency (EAF), Q-Q, and P-Z plot.

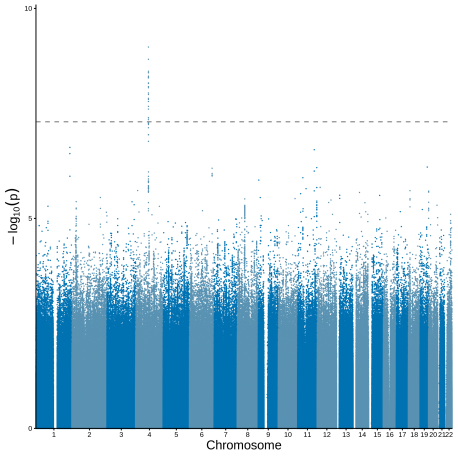


**(a)** Manhattan plot for 4-methyl-2-oxopentanoate (GCST90199655)

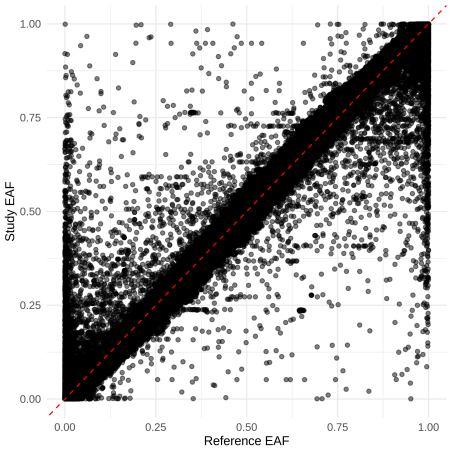


**(b)** EAF plot for 4-methyl-2-oxopentanoate (GCST90199655)

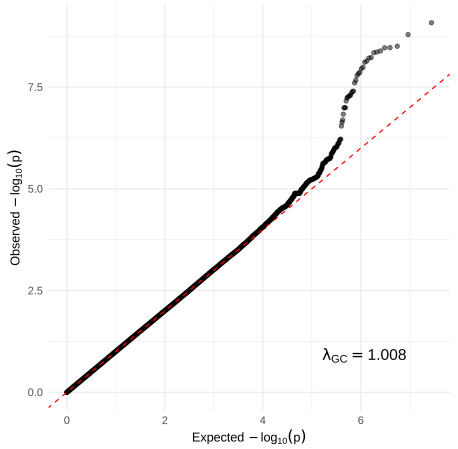


**(c)** Q-Q plot for 4-methyl-2-oxopentanoate (GCST90199655)

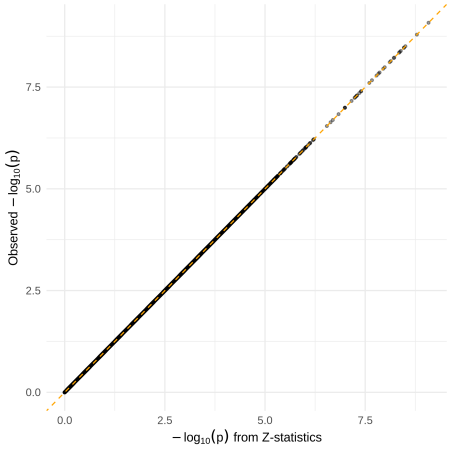


**(d)** P-Z plot for 4-methyl-2-oxopentanoate (GCST90199655)

**Figure A.5:** Quality control plots for the GWAS dataset of 4-methyl-2-oxopentanoate (GCST90199655), including Manhattan, effect allele frequency (EAF), Q-Q, and P-Z plot.

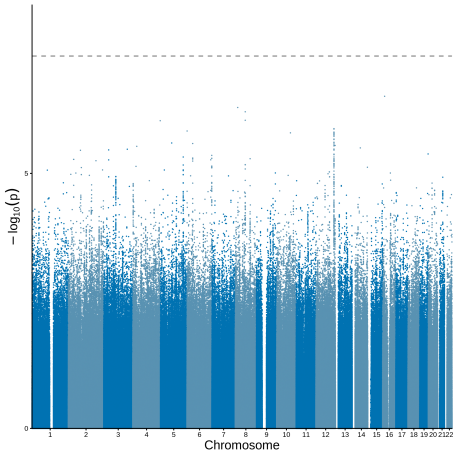


**(a)** Manhattan plot for 4-methyl-2-oxopentanoate (GCST90615432)

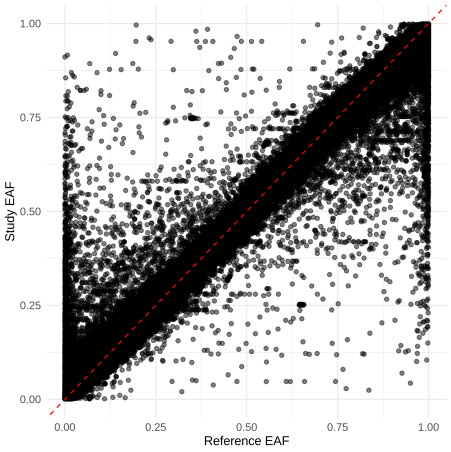


**(b)** EAF plot for 4-methyl-2-oxopentanoate (GCST90615432)

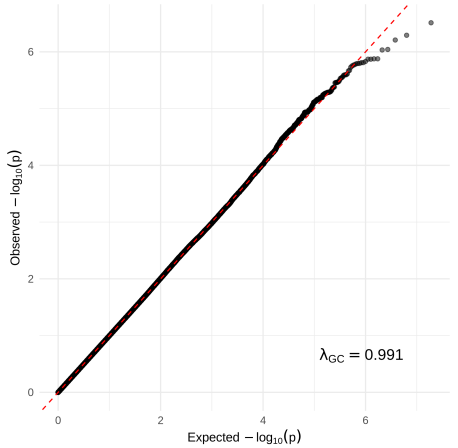


**(c)** Q-Q plot for 4-methyl-2-oxopentanoate (GCST90615432)

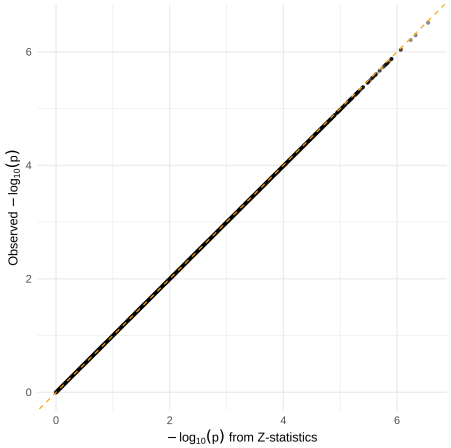


**(d)** P-Z plot for 4-methyl-2-oxopentanoate (GCST90615432)

**Figure A.6:** Quality control plots for the GWAS dataset of 4-methyl-2-oxopentanoate (GCST90615432), including Manhattan, effect allele frequency (EAF), Q-Q, and P-Z plot.

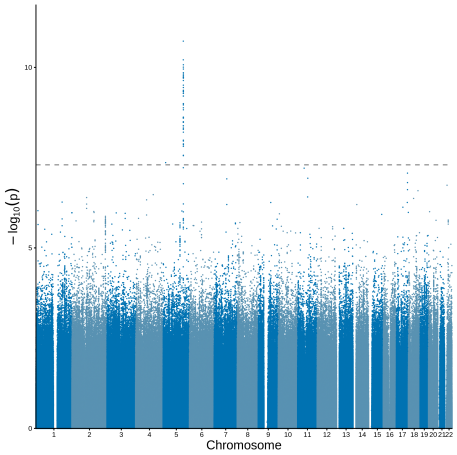


**(a)** Manhattan plot for oxalate (GCST90199672)

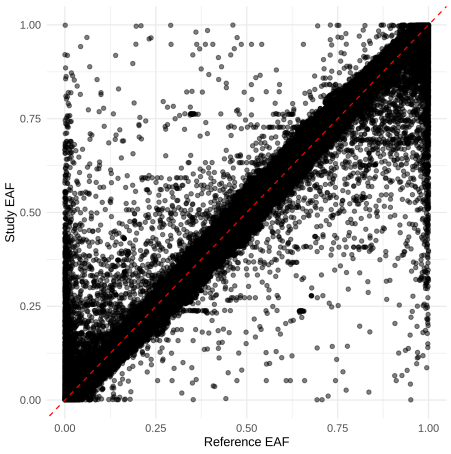


**(b)** EAF plot for oxalate (GCST90199672)

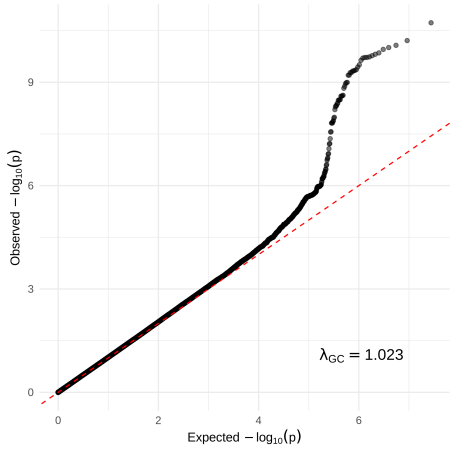


**(c)** Q-Q plot for oxalate (GCST90199672)

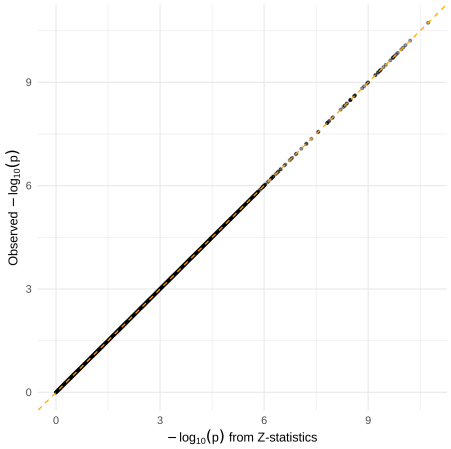


**(d)** P-Z plot for oxalate (GCST90199672)

**Figure A.7:** Quality control plots for the GWAS dataset of oxalate (GCST90199672), including Manhattan, effect allele frequency (EAF), Q-Q, and P-Z plot.

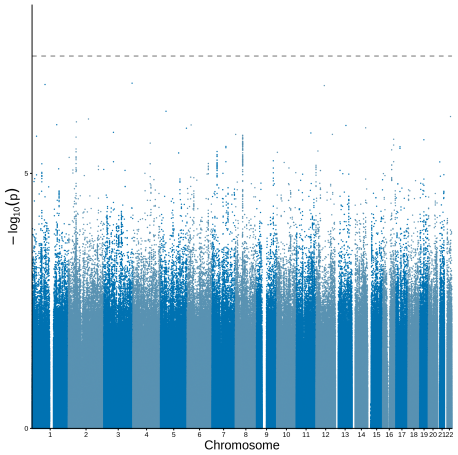


**(a)** Manhattan plot for oxalate (GCST90615459)

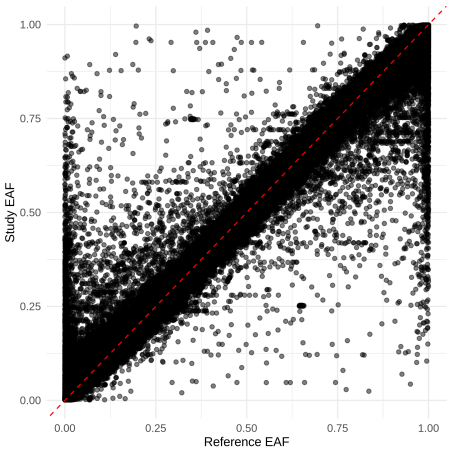


**(b)** EAF plot for oxalate (GCST90615459)

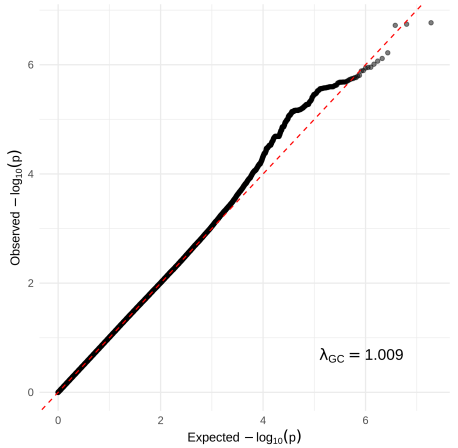


**(c)** Q-Q plot for oxalate (GCST90615459)

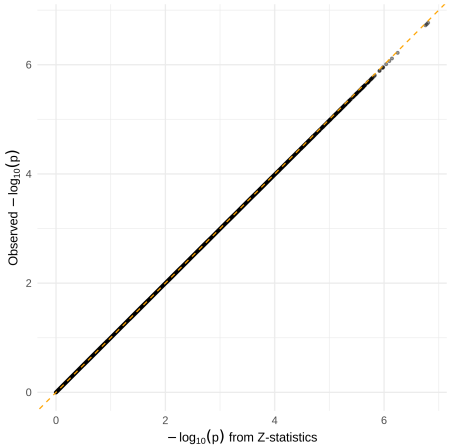


**(d)** P-Z plot for oxalate (GCST90615459)

**Figure A.8:** Quality control plots for the GWAS dataset of oxalate (GCST90615459), including Manhattan, effect allele frequency (EAF), Q-Q, and P-Z plot.

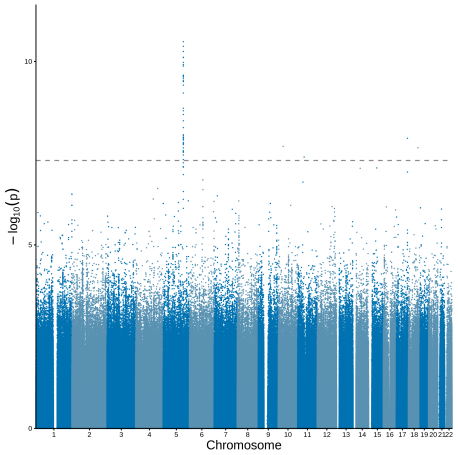


**(a)** Manhattan plot for threonate (GCST90199687)

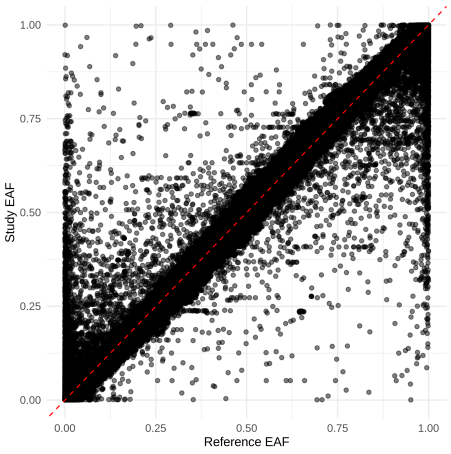


**(b)** EAF plot for threonate (GCST90199687)

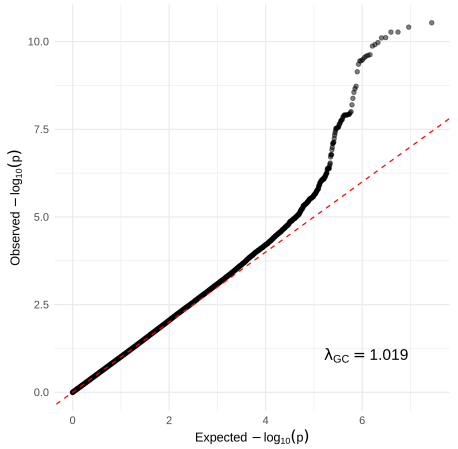


**(c)** Q-Q plot for threonate (GCST90199687)

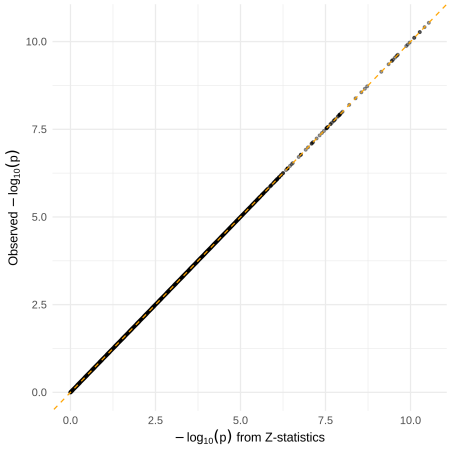


**(d)** P-Z plot for threonate (GCST90199687)

**Figure A.9:** Quality control plots for the GWAS dataset of threonate (GCST90199687), including Manhattan, effect allele frequency (EAF), Q-Q, and P-Z plot.

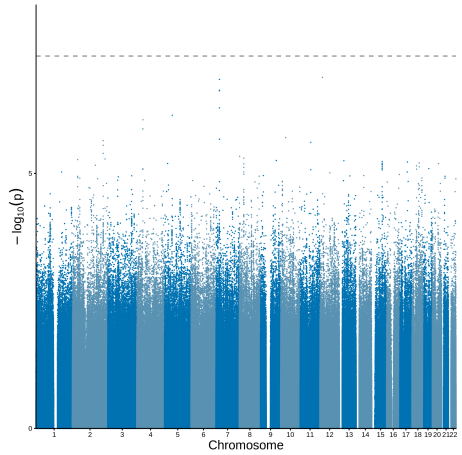


**(a)** Manhattan plot for threonate (GCST90615476)

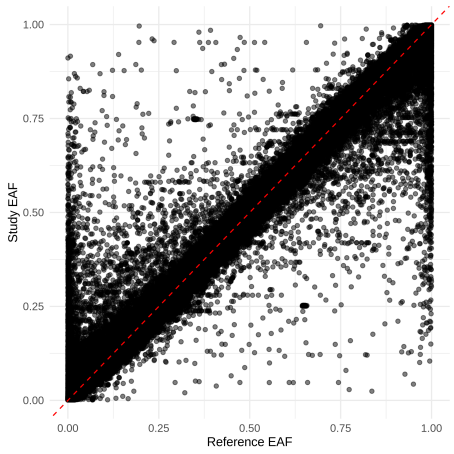


**(b)** EAF plot for threonate (GCST90615476)

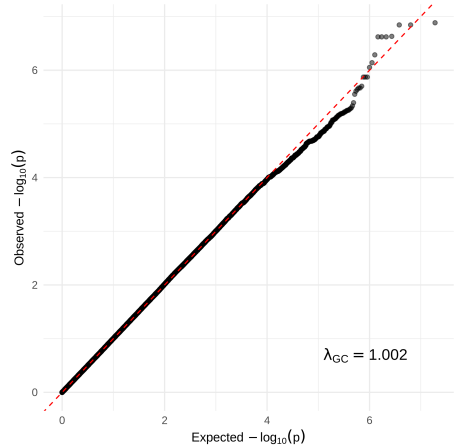


**(c)** Q-Q plot for threonate (GCST90615476)

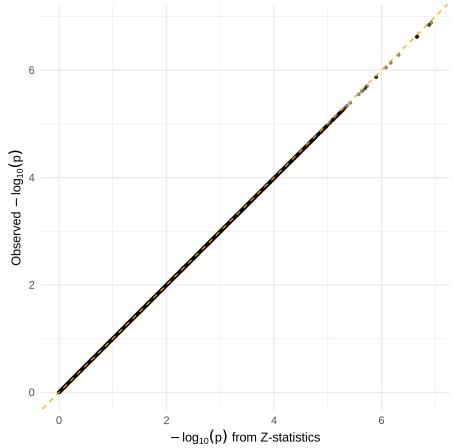


**(d)** P-Z plot for threonate (GCST90615476)

**Figure A.10:** Quality control plots for the GWAS dataset of threonate (GCST90615476), including Manhattan, effect allele frequency (EAF), Q-Q, and P-Z plot.

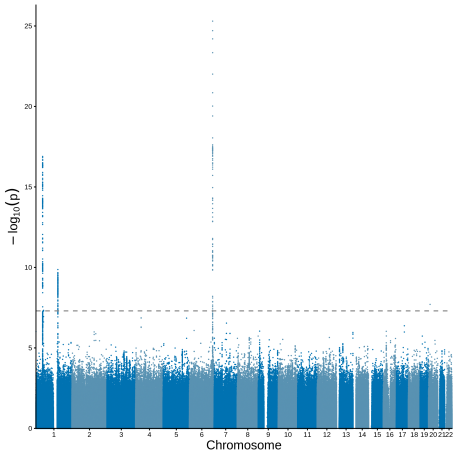


**(a)** Manhattan plot for pimeloylcarnitine (GCST90200101)

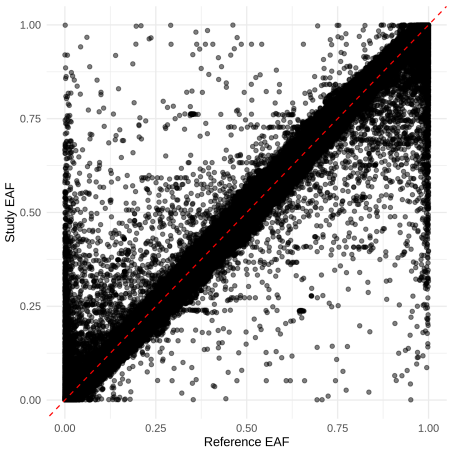


**(b)** EAF plot for pimeloylcarnitine (GCST90200101)

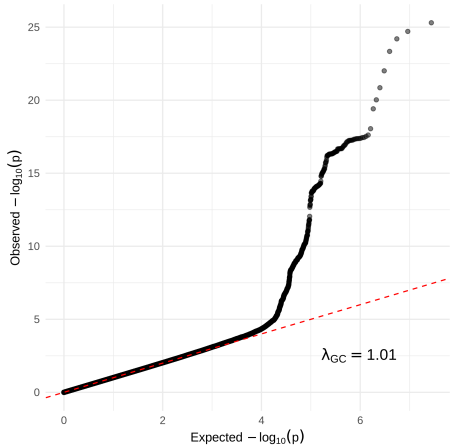


**(c)** Q-Q plot for pimeloylcarnitine (GCST90200101)

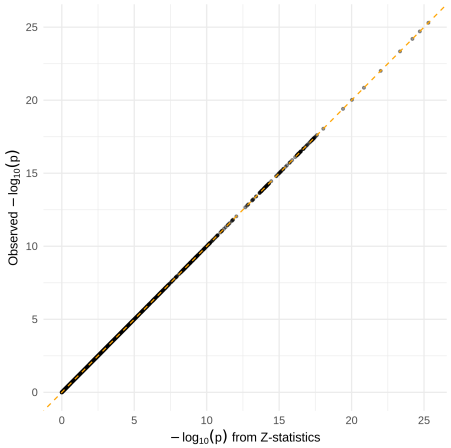


**(d)** P-Z plot for pimeloylcarnitine (GCST90200101)

**Figure A.11:** Quality control plots for the GWAS dataset of pimeloylcarnitine (GCST90200101), including Manhattan, effect allele frequency (EAF), Q-Q, and P-Z plot.

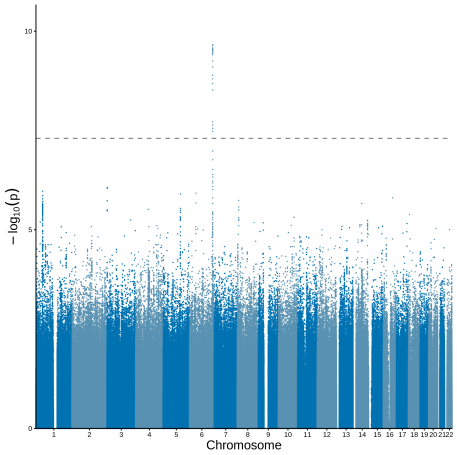


**(a)** Manhattan plot for pimeloylcarnitine (GCST90616070)

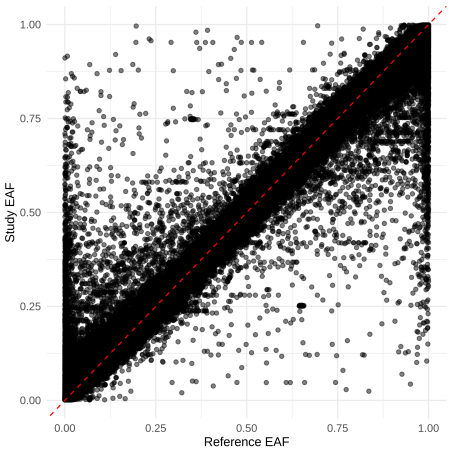


**(b)** EAF plot for pimeloylcarnitine (GCST90616070)

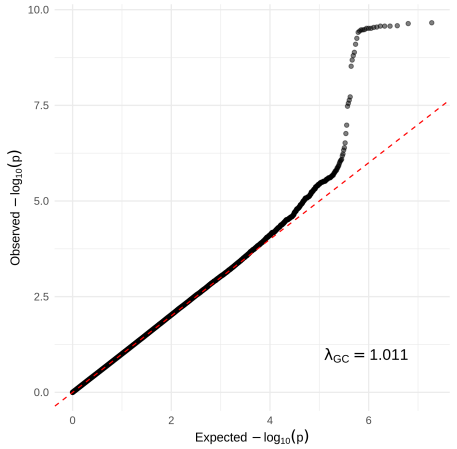


**(c)** Q-Q plot for pimeloylcarnitine (GCST90616070)

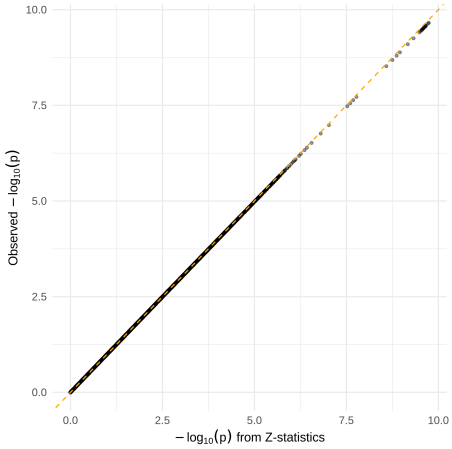


**(d)** P-Z plot for pimeloylcarnitine (GCST90616070)

**Figure A.12:** Quality control plots for the GWAS dataset of pimeloylcarnitine (GCST90616070), including Manhattan, effect allele frequency (EAF), Q-Q, and P-Z plot.

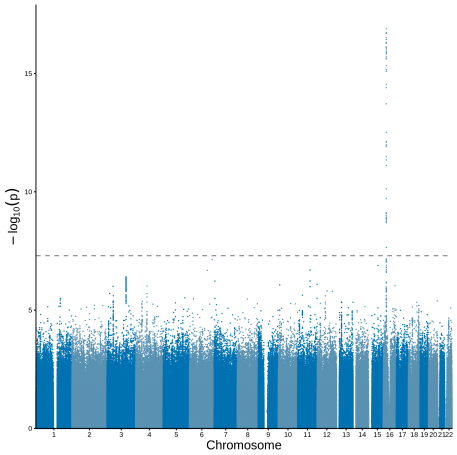


**(a)** Manhattan plot for phenylacetate (GCST90199630)

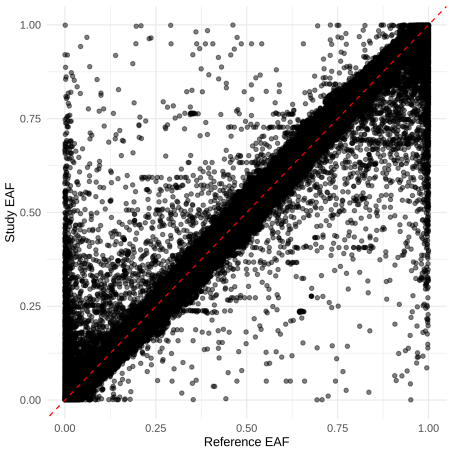


**(b)** EAF plot for phenylacetate (GCST90199630)

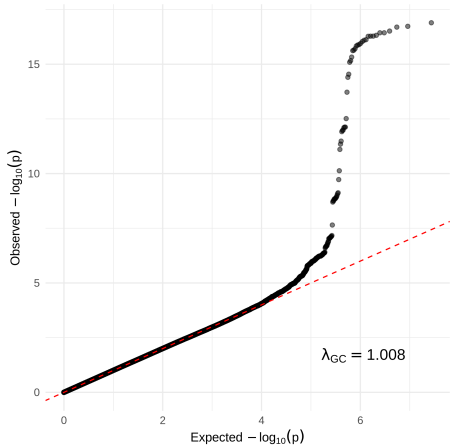


**(c)** Q-Q plot for phenylacetate (GCST90199630)

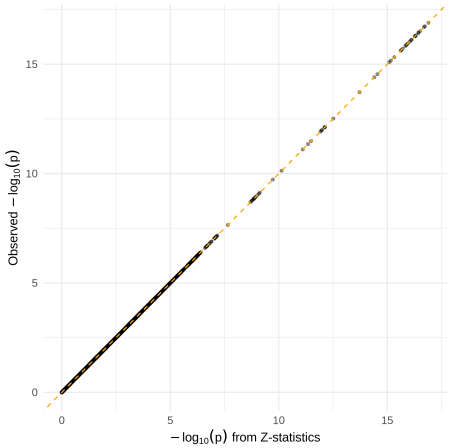


**(d)** P-Z plot for phenylacetate (GCST90199630)

**Figure A.13:** Quality control plots for the GWAS dataset of phenylacetate (GCST90199630), including Manhattan, effect allele frequency (EAF), Q-Q, and P-Z plot.

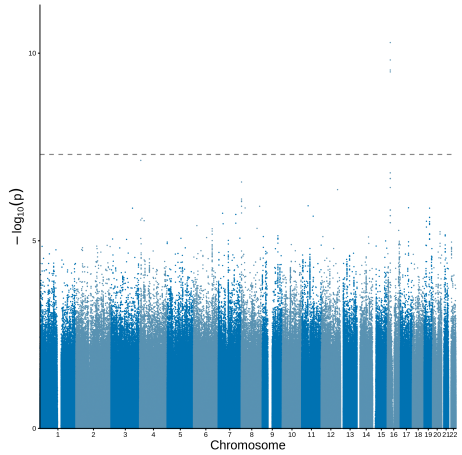


**(a)** Manhattan plot for phenylacetate (GCST90615403)

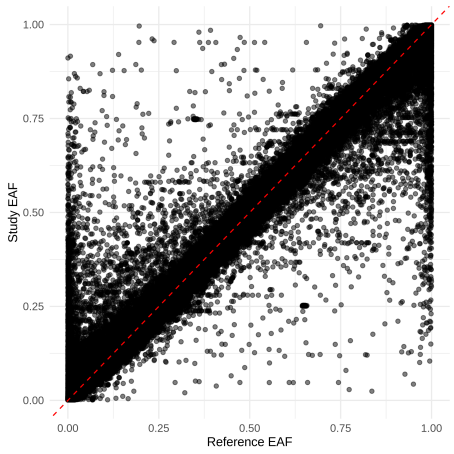


**(b)** EAF plot for phenylacetate (GCST90615403)

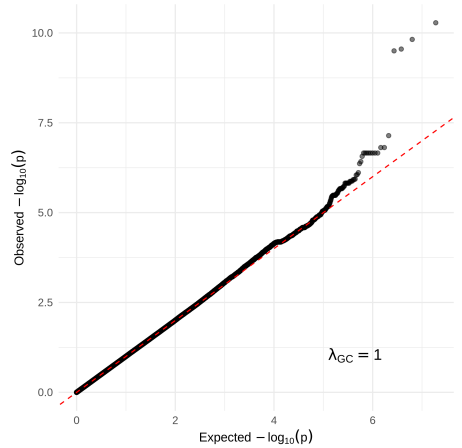


**(c)** Q-Q plot for phenylacetate (GCST90615403)

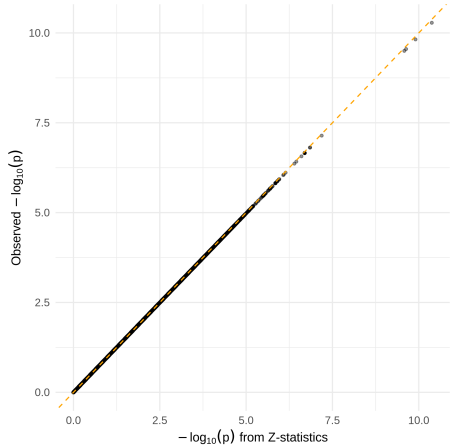


**(d)** P-Z plot for phenylacetate (GCST90615403)

**Figure A.14:** Quality control plots for the GWAS dataset of phenylacetate (GCST90615403), including Manhattan, effect allele frequency (EAF), Q-Q, and P-Z plot.

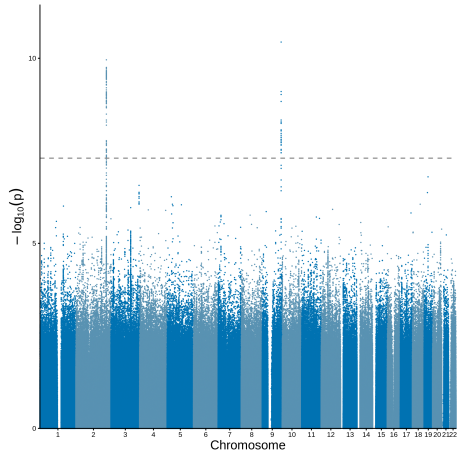


**(a)** Manhattan plot for citrulline (GCST90200403)

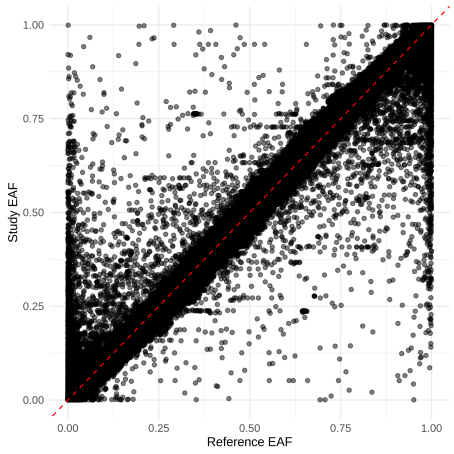


**(b)** EAF plot for citrulline (GCST90200403)

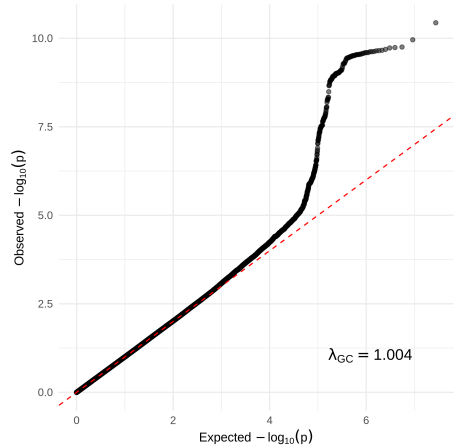


**(c)** Q-Q plot for citrulline (GCST90200403)

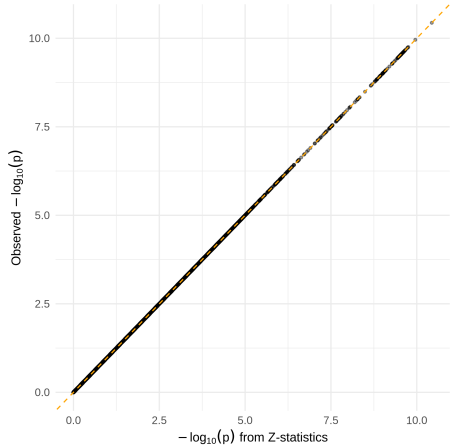


**(d)** P-Z plot for citrulline (GCST90200403)

**Figure A.15:** Quality control plots for the GWAS dataset of citrulline (GCST90200403), including Manhattan, effect allele frequency (EAF), Q-Q, and P-Z plot.

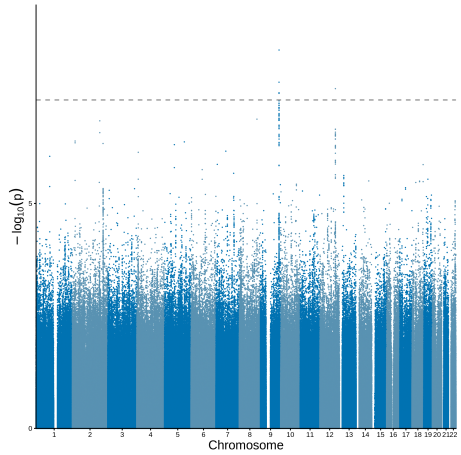


**(a)** Manhattan plot for citrulline (GCST90616468)

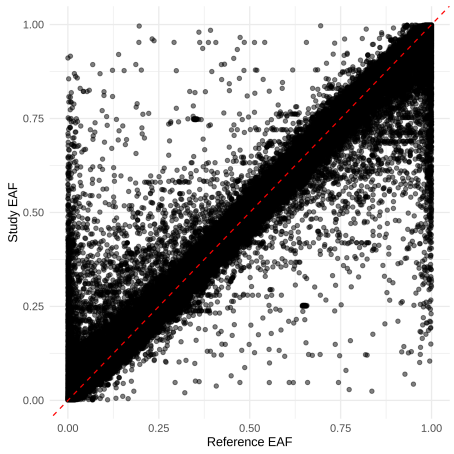


**(b)** EAF plot for citrulline (GCST90616468)

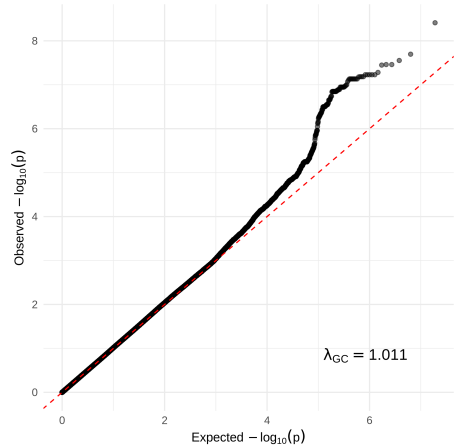


**(c)** Q-Q plot for citrulline (GCST90616468)

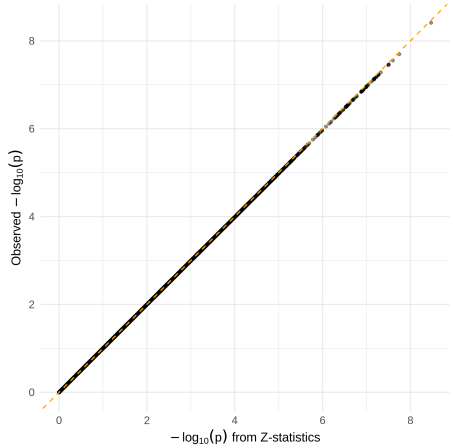


**(d)** P-Z plot for citrulline (GCST90616468)

**Figure A.16:** Quality control plots for the GWAS dataset of citrulline (GCST90616468), including Manhattan, effect allele frequency (EAF), Q-Q, and P-Z plot.

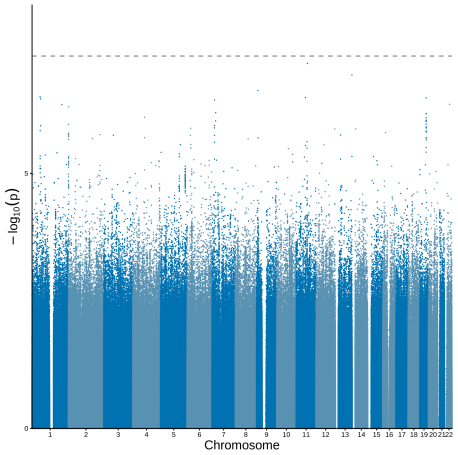


**(a)** Manhattan plot for maltose (GCST90200447)

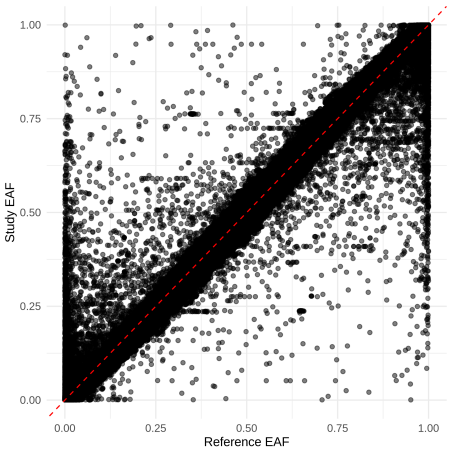


**(b)** EAF plot for maltose (GCST90200447)

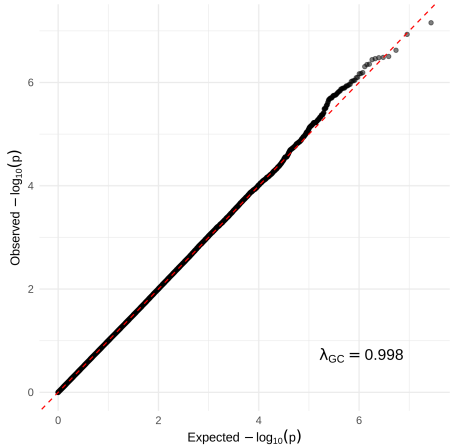


**(c)** Q-Q plot for maltose (GCST90200447)

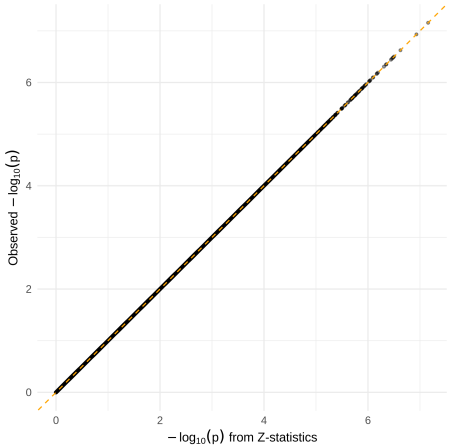


**(d)** P-Z plot for maltose (GCST90200447)

**Figure A.17:** Quality control plots for the GWAS dataset of maltose (GCST90200447), including Manhattan, effect allele frequency (EAF), Q-Q, and P-Z plot.

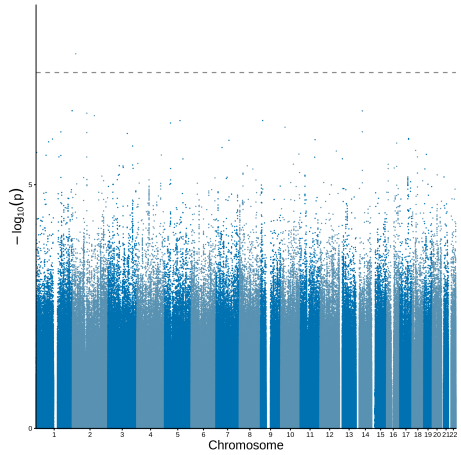


**(a)** Manhattan plot for maltose (GCST90616526)

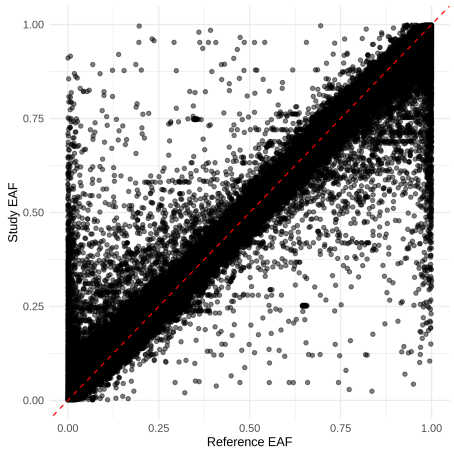


**(b)** EAF plot for maltose (GCST90616526)

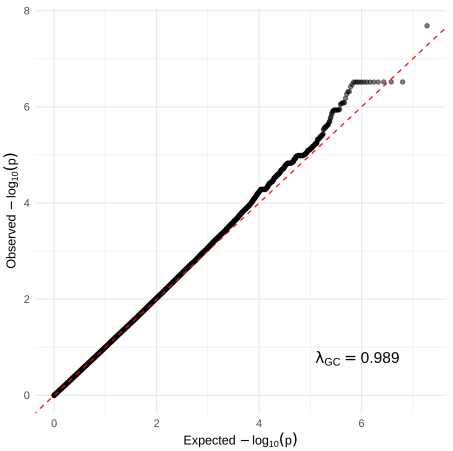


**(c)** Q-Q plot for maltose (GCST90616526)

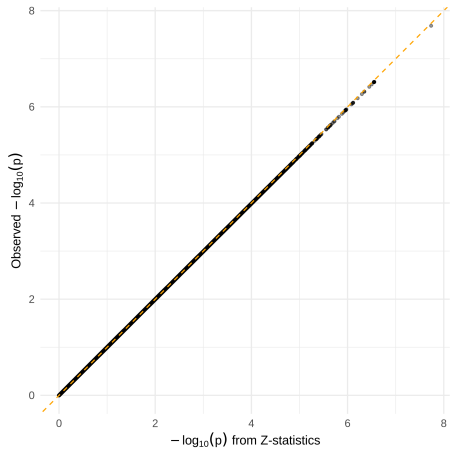


**(d)** P-Z plot for maltose (GCST90616526)

**Figure A.18:** Quality control plots for the GWAS dataset of maltose (GCST90616526), including Manhattan, effect allele frequency (EAF), Q-Q, and P-Z plot.

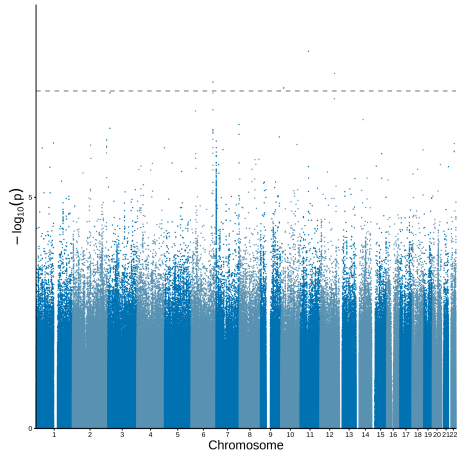


**(a)** Manhattan plot for arabinose (GCST90616516)

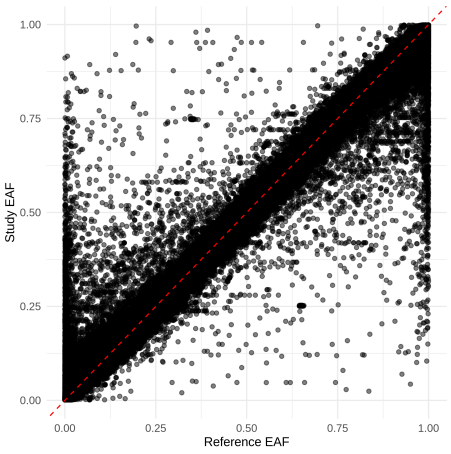


**(b)** EAF plot for arabinose (GCST90616516)

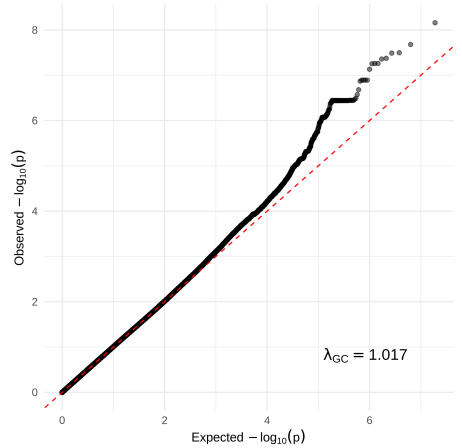


**(c)** Q-Q plot for arabinose (GCST90616516)

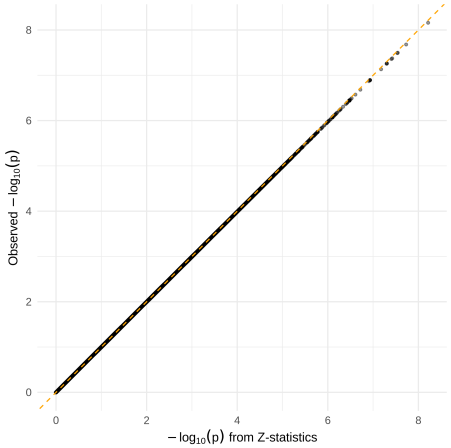


**(d)** P-Z plot for arabinose (GCST90616516)

**Figure A.19:** Quality control plots for the GWAS dataset of arabinose (GCST90616516), including Manhattan, effect allele frequency (EAF), Q-Q, and P-Z plot.

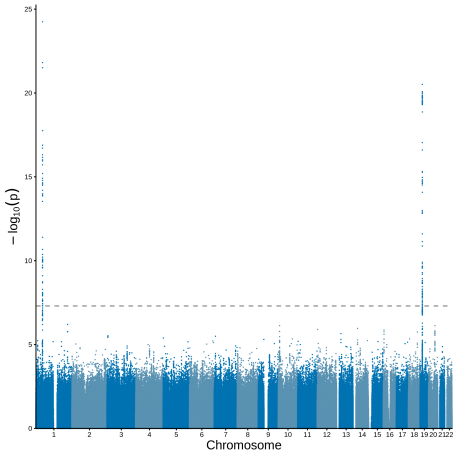


**(a)** Manhattan plot for succinoyltaurine (GCST90616288)

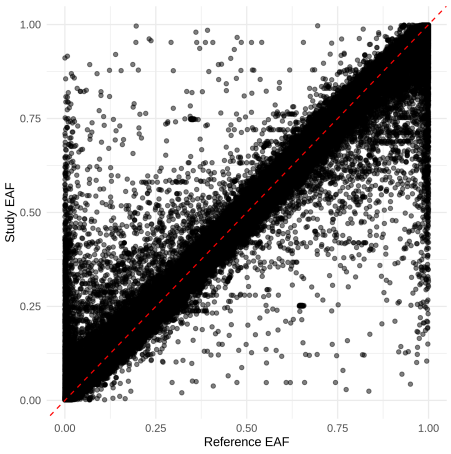


**(b)** EAF plot for succinoyltaurine (GCST90616288)

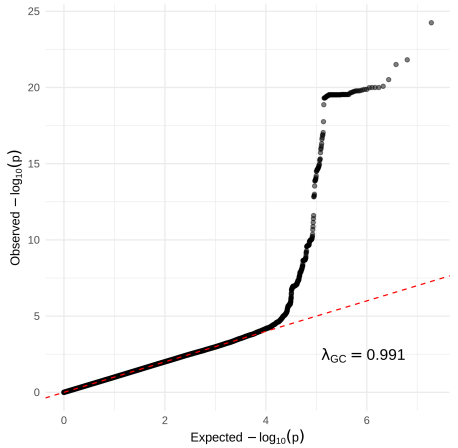


**(c)** Q-Q plot for succinoyltaurine (GCST90616288)

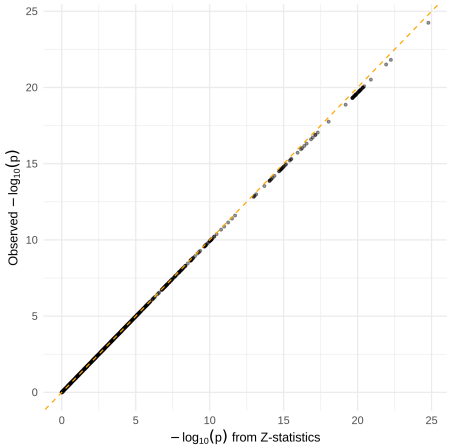


**(d)** P-Z plot for succinoyltaurine (GCST90616288)

**Figure A.20:** Quality control plots for the GWAS dataset of succinoyltaurine (GCST90616288), including Manhattan, effect allele frequency (EAF), Q-Q, and P-Z plot.

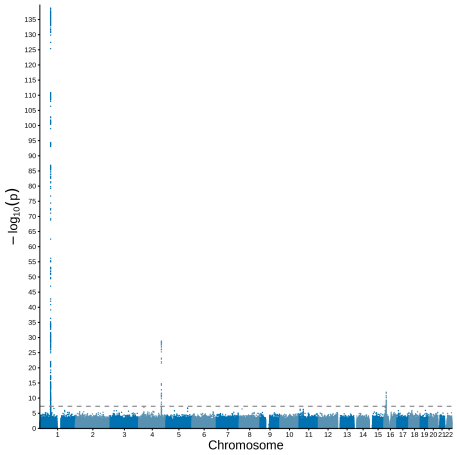


**(a)** Manhattan plot for octanoylcarnitine (GCST90199720)

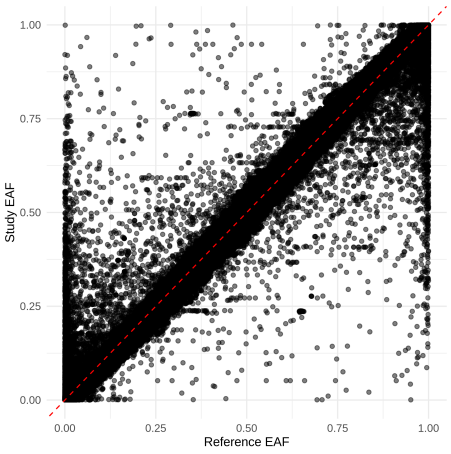


**(b)** EAF plot for octanoylcarnitine (GCST90199720)

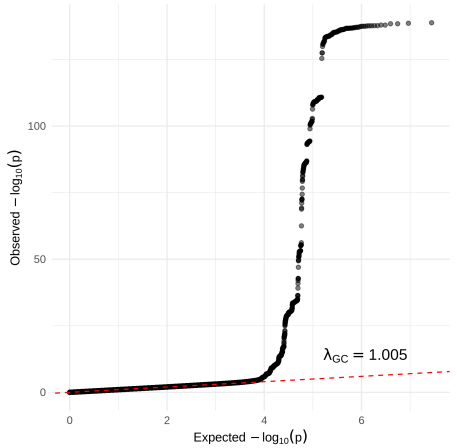


**(c)** Q-Q plot for octanoylcarnitine (GCST90199720)

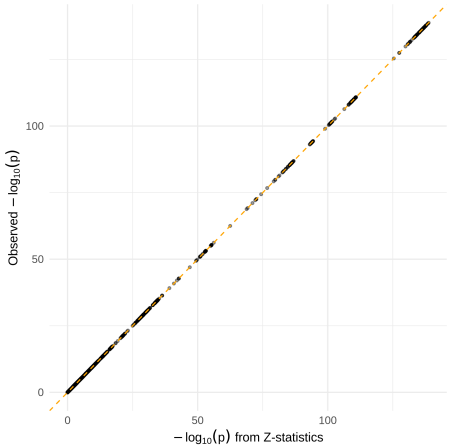


**(d)** P-Z plot for octanoylcarnitine (GCST90199720)

**Figure A.21:** Quality control plots for the GWAS dataset of octanoylcarnitine (GCST90199720), including Manhattan, effect allele frequency (EAF), Q-Q, and P-Z plot.

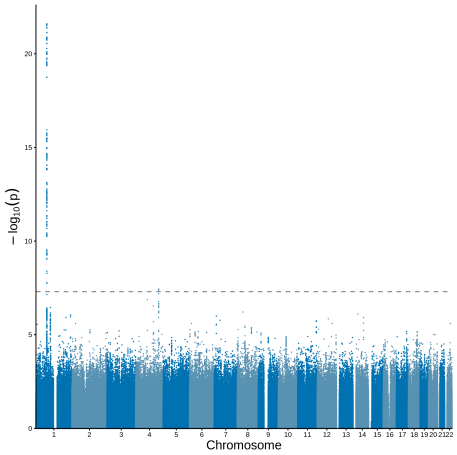


**(a)** Manhattan plot for octanoylcarnitine (GCST90615518)

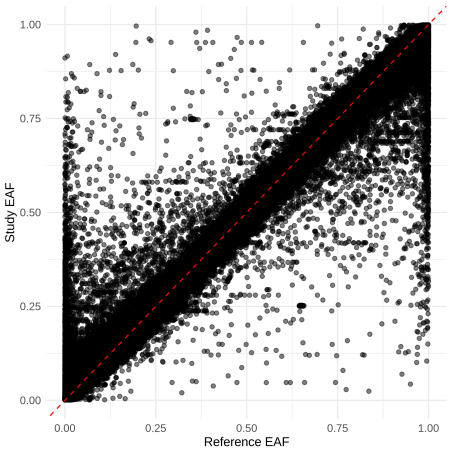


**(b)** EAF plot for octanoylcarnitine (GCST90615518)

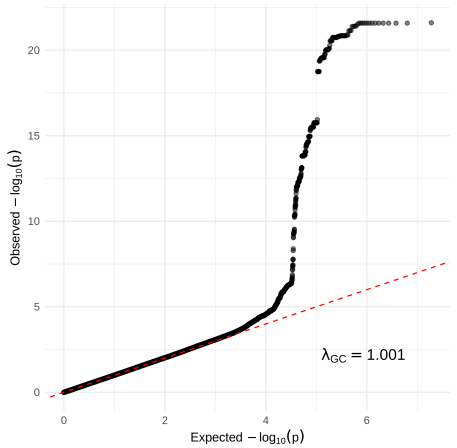


**(c)** Q-Q plot for octanoylcarnitine (GCST90615518)

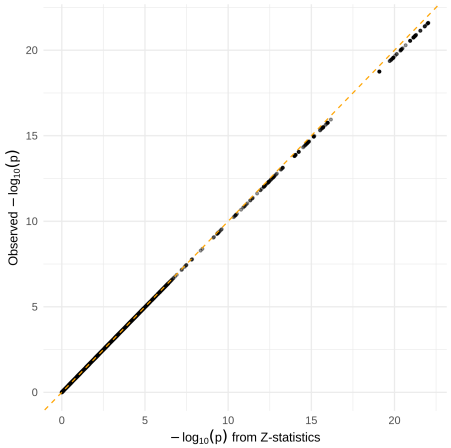


**(d)** P-Z plot for octanoylcarnitine (GCST90615518)

**Figure A.22:** Quality control plots for the GWAS dataset of octanoylcarnitine (GCST90615518), including Manhattan, effect allele frequency (EAF), Q-Q, and P-Z plot.

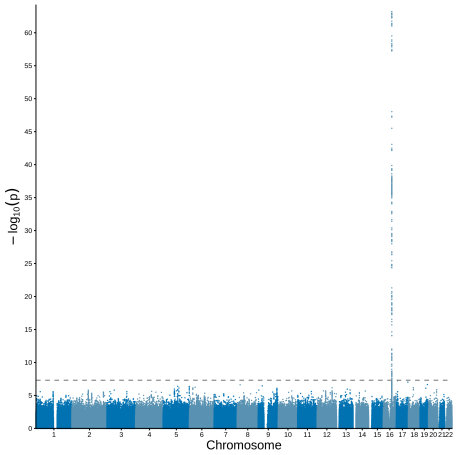


**(a)** Manhattan plot for phenyllactate (GCST90199664)

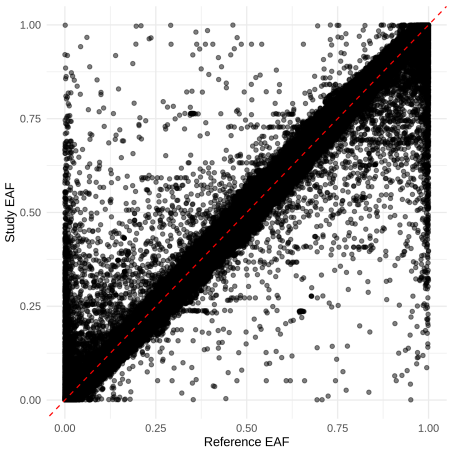


**(b)** EAF plot for phenyllactate (GCST90199664)

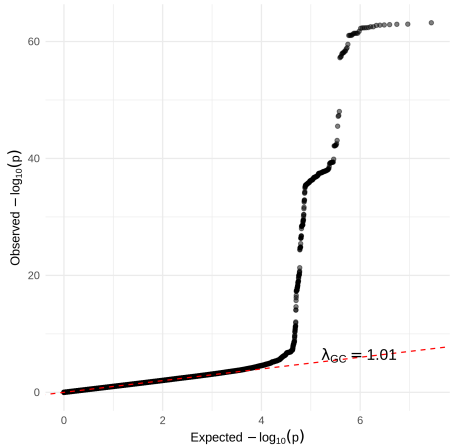


**(c)** Q-Q plot for phenyllactate (GCST90199664)

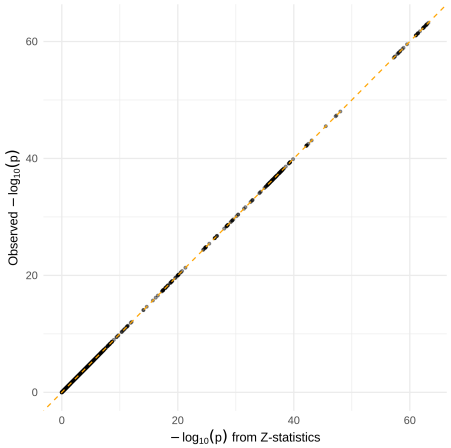


**(d)** P-Z plot for phenyllactate (GCST90199664)

**Figure A.23:** Quality control plots for the GWAS dataset of phenyllactate (GCST90199664), including Manhattan, effect allele frequency (EAF), Q-Q, and P-Z plot.

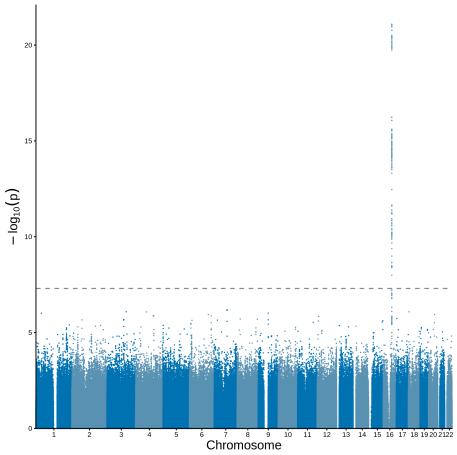


**(a)** Manhattan plot for phenyllactate (GCST90615449)

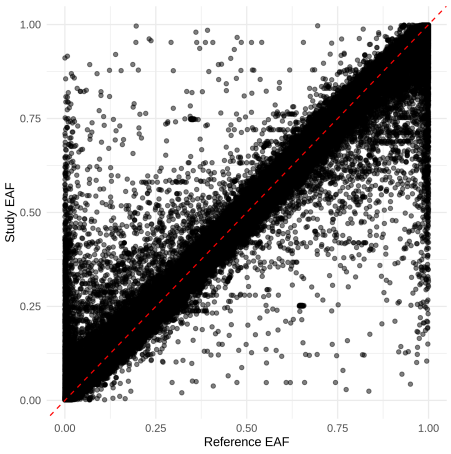


**(b)** EAF plot for phenyllactate (GCST90615449)

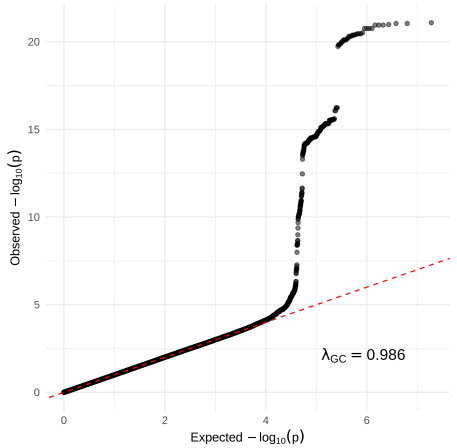


**(c)** Q-Q plot for phenyllactate (GCST90615449)

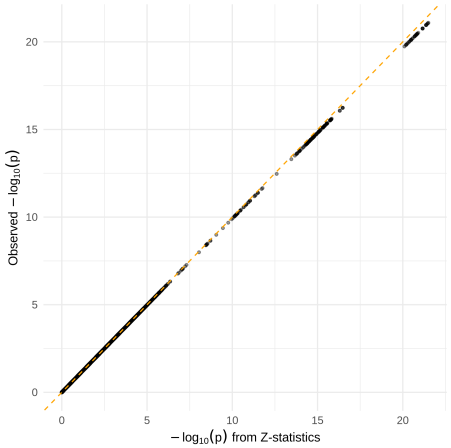


**(d)** P-Z plot for phenyllactate (GCST90615449)

**Figure A.24:** Quality control plots for the GWAS dataset of phenyllactate (GCST90615449), including Manhattan, effect allele frequency (EAF), Q-Q, and P-Z plot.

## A.2 Non-associated metabolites

## A.3 PSC

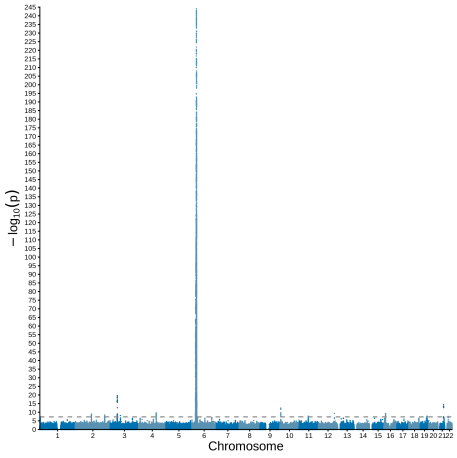


**(a)** Manhattan plot for PSC (GCST004030)

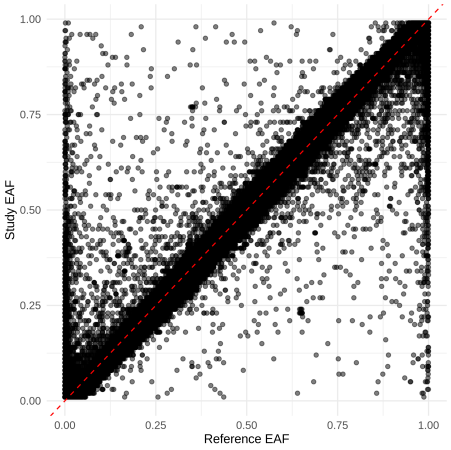


**(b)** EAF plot for PSC (GCST004030)

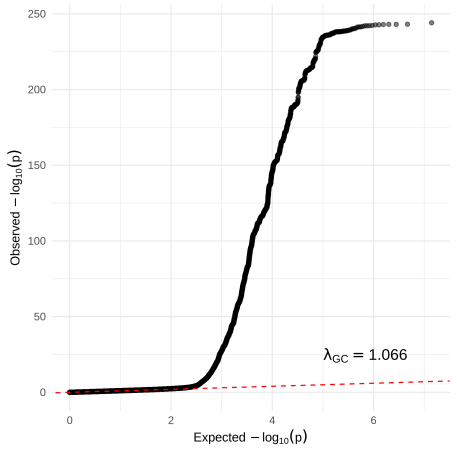


**(c)** Q-Q plot for PSC (GCST004030)

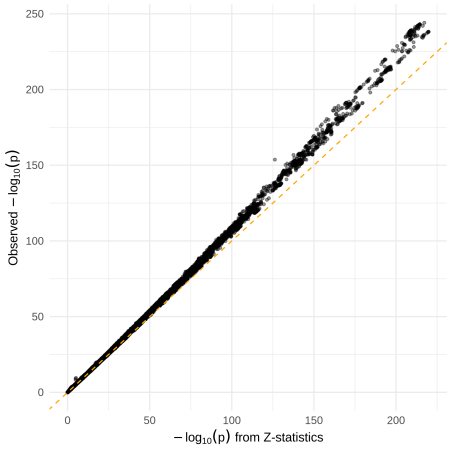


**(d)** P-Z plot for PSC (GCST004030)

**Figure A.25:** Quality control plots for the GWAS dataset of PSC (GCST004030), including Manhattan, effect allele frequency (EAF), Q-Q, and P-Z plot.

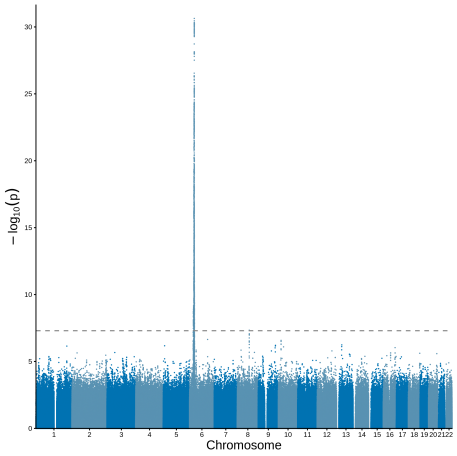


**(a)** Manhattan plot for PSC (finngen_R12_K11_PSC_COLITIS_STRICT)

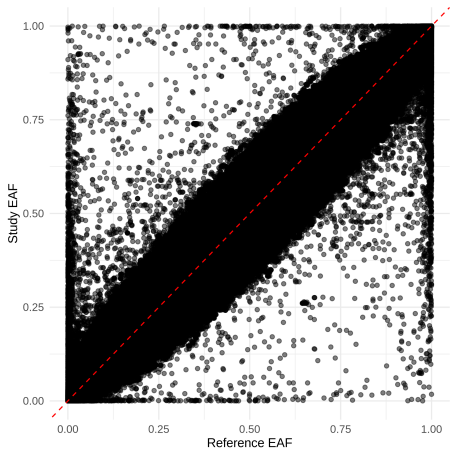


**(b)** EAF plot for PSC (finngen_R12_K11_PSC_COLITIS_STRICT)

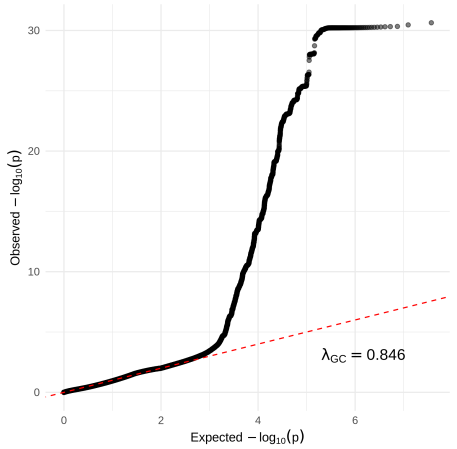


**(c)** Q-Q plot for PSC (finngen_R12_K11_PSC_COLITIS_STRICT)

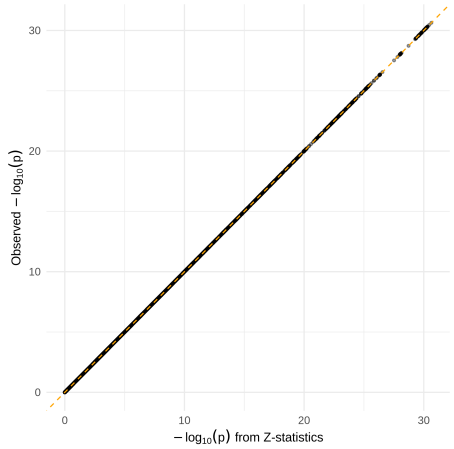


**(d)** P-Z plot for PSC (finngen_R12_K11_PSC_COLITIS_STRICT)

**Figure A.26:** Quality control plots for the GWAS dataset of PSC (finngen_R12_K11_PSC_COLITIS_STRICT), including Manhattan, effect allele frequency (EAF), Q-Q, and P-Z plot.

# B

# Instrumental variable quality

## B.1 PSC-associated metabolites

**Table B.1:** F-statistics for individual SNPs in each of the PSC-associated metabolites.

| Metabolite | ID | SNP | F-statistic |
|---|---|---|---|
| Imidazole propionate | GCST90199915 | 1:177789561:T:C | 0.037 |
| | | 12:242301:G:A | 1.767 |
| Oxalate | GCST90199672 | 5:138843482:T:C | 1.866 |
| Threonate | GCST90199687 | 11:44829113:T:C | 0.174 |
| | | 17:76864313:G:A | 1.903 |
| | | 5:139350290:T:G | 0.036 |
| Pimeloylcarnitine | GCST90200101 | 1:151931670:T:A | 0.551 |
| | | 1:46923941:T:C | 0.542 |
| | | 1:53208870:G:A | 1.018 |
| | | 20:10779055:T:C | 0.303 |
| | | 6:160122116:T:C | 0.172 |
| | | 6:160139792:G:A | 0.557 |
| | | 6:160146896:T:G | 4.835 |
| | GCST90616070 | 6:160075211:T:G | 0.339 |

## B.2 Non-associated metabolites

**Table B.2:** F-statistics for individual SNPs in each of the non-associated metabolites.

| Metabolite | ID | SNP | F-statistic |
|---|---|---|---|
| Arabinose | | 10:20746016:G:A | 1.496 |
| | | 11:57006465:G:A | 0.276 |
| | | 12:99849814:T:G | 4.952 |
| | | 6:150028194:T:C | 1.694 |
| Succinoyltaurine | | 1:46405089:C:A | 0.032 |
| | | 19:15875578:G:A | 2.074 |
| Octanoylcarnitine | | 1:75758325:T:C | 0.023 |
| | | 1:75761161:G:A | 1.281 |
| | | 1:75767505:T:C | 2.773 |
| | | 16:16001985:T:G | 0.009 |
| | | 4:158713764:T:C | 1.016 |
| Phenylacetate | | 16:20543220:G:A | 0.953 |
| | | 16:20544152:T:C | 0.064 |
| Citrulline | | 2:210564791:G:A | 0.009 |
| | | 9:127198873:T:C | 0.026 |
| Phenyllactate | | 16:58742952:T:C | 1.983 |
| | | 16:58830687:T:G | 0.012 |

# C

# Sensitivity analysis

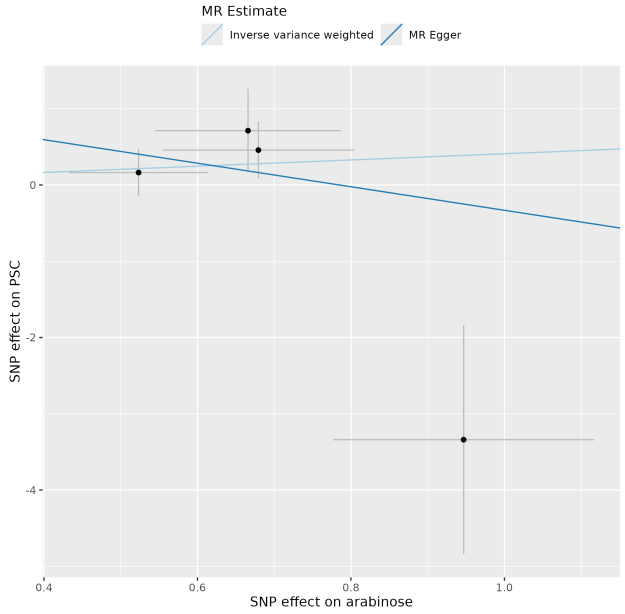


**Figure C.1:** Scatter plot with MR-Egger and IVW regression for arabinose.

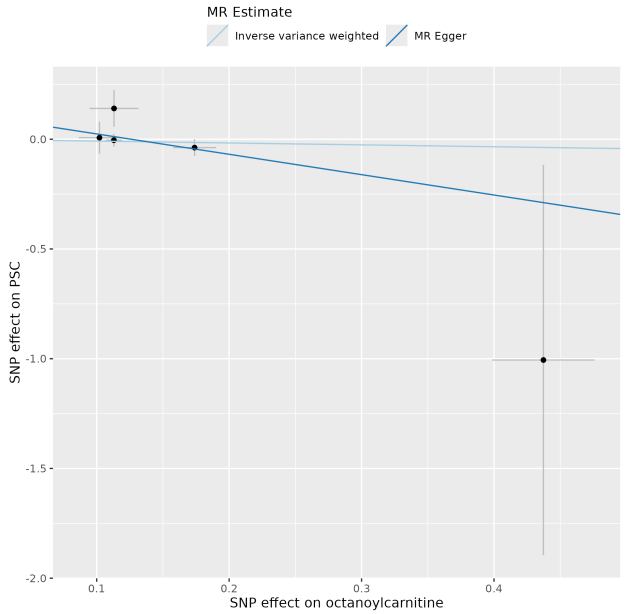


**Figure C.2:** Scatter plot with MR-Egger and IVW regression for octanoylcarnitine.

**DEPARTMENT OF LIFE SCIENCES**
**CHALMERS UNIVERSITY OF TECHNOLOGY**
Gothenburg, Sweden
www.chalmers.se


CHALMERS
UNIVERSITY OF TECHNOLOGY